Article

Synthesis, Characterization, and Transistor Response of Semiconducting Silole Polymers with Substantial Hole Mobility and Air Stability. Experiment and Theory

Gang Lu, Hakan Usta, Chad Risko, Lian Wang, Antonio Facchetti, Mark A. Ratner, and Tobin J. Marks

J. Am. Chem. Soc., **2008**, 130 (24), 7670-7685 • DOI: 10.1021/ja800424m • Publication Date (Web): 28 May 2008

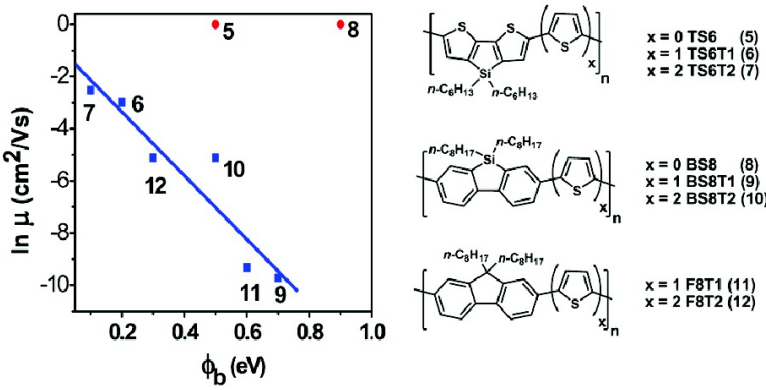

More About This Article

Additional resources and features associated with this article are available within the HTML version:

- Supporting Information
- Links to the 4 articles that cite this article, as of the time of this article download
- Access to high resolution figures
- Links to articles and content related to this article
- Copyright permission to reproduce figures and/or text from this article

View the Full Text HTML

J|A|C|S
ARTICLES

Published on Web 05/28/2008

Synthesis, Characterization, and Transistor Response of Semiconducting Silole Polymers with Substantial Hole Mobility and Air Stability. Experiment and Theory

Gang Lu, Hakan Usta, Chad Risko, Lian Wang, Antonio Facchetti,* Mark A. Ratner,* and Tobin J. Marks*

Department of Chemistry and the Materials Research Center, Northwestern University, 2145 Sheridan Road, Evanston, Illinois 60208

Received February 11, 2008; E-mail: a-facchetti@northwestern.edu; t-marks@northwestern.edu; ratner@northwestern.edu

Abstract: Realizing p-channel semiconducting polymers with good hole mobility, solution processibility, and air stability is an important step forward in the chemical manipulation of charge transport in polymeric solids and in the development of low-cost printed electronics. We report here the synthesis and full characterization of the dithienosilole- and dibenzosilole-based homopolymers, poly(4,4-di-*n*-hexyldithienosilole) (**TS6**) and poly(9,9-di-*n*-octyldibenzosilole) (**BS8**), and their mono- and bithiophene copolymers, poly(4,4-di-*n*-hexyldithienosilole-*alt*-(bi)thiophene) (**TS6T1**,**TS6T2**) and poly(9,9-di-*n*-octyldibenzosilole-*alt*-(bi)thiophene) (**BS8T1**,**BS8T2**), and examine in detail the consequences of introducing dithienosilole and dibenzosilole cores into a thiophene polymer backbone. We demonstrate air-stable thin-film transistors (TFTs) fabricated under ambient conditions having hole mobilities as large as 0.08 $cm^2/V \cdot s$, low turn-on voltages, and current on/off ratios $> 10^6$. Additionally, unencapsulated TFTs fabricated under ambient conditions are air-stable, an important advance over regioregular poly(3-hexylthiophene) (P3HT)-based devices. Density functional theory calculations provide detailed insight into the polymer physicochemical and charge transport characteristics. A direct correlation between the hole injection barrier and both TFT turn-on voltage and TFT polymer hole mobility is identified and discussed, in combination with thin-film morphological characteristics, to explain the observed OTFT performance trends.

Introduction

π-Conjugated oligomeric and polymeric semiconductors have been the focus of intense research over the past few decades as alternatives to inorganic semiconductors for low-cost electronic applications such as organic thin-film transistors (OTFTs),[1–4] light-emitting diodes (OLEDs),[5,6] and photovoltaics (OPVs).[7–10] These materials enable vapor- or solution-phase fabrication of large-area, lightweight electronic devices and are compatible with plastic substrates for mechanically flexible, conformable, and wearable electronics. OTFTs can be used in low-performance memory elements, sensors, and drive electronics for active-matrix displays.[11,12] OLEDs are envisioned as cheap, energy-efficient alternatives to liquid crystal displays and solid-state lighting sources. Flat-panel displays based on OLEDs are emerging in commercial portable electronic devices and novel textiles.

Among the organic semiconductor classes used for OTFTs, (oligo, poly)-thiophenes have been among the most extensively investigated. The hole transporting properties of α-sexithiophene ($\alpha-6T$) were first disclosed in 1988,[13] and p-type OTFTs fabricated from thermally evaporated $\alpha-6T$ thin films were reported one year later.[14,15] High-performance electron-transporting (n-type) oligothiophenes have also been developed to fully realize the potential of organic electronics via complementary circuits.[16–18] Unfortunately, OTFTs based on oligothiophenes usually exhibit lower mobilities when films are grown

(1) Murphy, A. R.; Frechet, J. M. J. *Chem. Rev.* **2007**, *107*, 1066–1096.
(2) Facchetti, A. *Mater. Today* **2007**, *10*, 28.
(3) Dimitrakopoulos, C. D.; Malenfant, P. R. L. *Adv. Mater.* **2002**, *14*, 99–117.
(4) Katz, H. E. *Chem. Mater.* **2004**, *16*, 4748–4756.
(5) Bernius, M.; Inbasekaran, M.; Woo, E.; Wu, W. S.; Wujkowski, L. *Thin Solid Films* **2000**, *363*, 55–57.
(6) Kraft, A.; Grimsdale, A. C.; Holmes, A. B. *Angew. Chem., Intl. Ed.* **1998**, *37*, 402–428.
(7) Brabec, C. J.; Sariciftci, N. S.; Hummelen, J. C. *Adv. Funct. Mater.* **2001**, *11*, 15–26.
(8) Huynh, W. U.; Dittmer, J. J.; Alivisatos, A. P. *Science* **2002**, *295*, 2425–2427.
(9) Yu, G.; Gao, J.; Hummelen, J. C.; Wudl, F.; Heeger, A. J. *Science* **1995**, *270*, 1789–1791.
(10) Berlin, A.; Zotti, G.; Zecchin, S.; Schiavon, G.; Vercelli, B.; Zanelli, A. *Chem. Mater.* **2004**, *16*, 3667–3676.
(11) Huitema, H. E. A.; Gelinck, G. H.; van der Putten, J. B. P. H.; Kuijk, K. E.; Hart, K. M.; Cantatore, E.; de Leeuw, D. M. *Adv. Mater.* **2002**, *14*, 1201–1204.
(12) Mach, P.; Rodriguez, S. J.; Nortrup, R.; Wiltzius, P.; Rogers, J. A. *Appl. Phys. Lett.* **2001**, *78*, 3592–3594.
(13) Fichou, D.; Horowitz, G.; Nishikitani, Y.; Garnier, F. *Chemtronics* **1988**, *3*, 176–178.
(14) Horowitz, G.; Fichou, D.; Peng, X. Z.; Xu, Z. G.; Garnier, F. *Solid State Commun.* **1989**, *72*, 381–384.
(15) Peng, X. Z.; Horowitz, G.; Fichou, D.; Garnier, F. *Appl. Phys. Lett.* **1990**, *57*, 2013–2015.
(16) Facchetti, A.; Mushrush, M.; Yoon, M. H.; Hutchison, G. R.; Ratner, M. A.; Marks, T. J. *J. Am. Chem. Soc.* **2004**, *126*, 13859–13874.
(17) Facchetti, A.; Yoon, M. H.; Stern, C. L.; Hutchison, G. R.; Ratner, M. A.; Marks, T. J. *J. Am. Chem. Soc.* **2004**, *126*, 13480–13501.
(18) Facchetti, A.; Yoon, M. H.; Stern, C. L.; Katz, H. E.; Marks, T. J. *Angew. Chem., Intl. Ed.* **2003**, *42*, 3900–3903.

 10.1021/ja800424m CCC: $40.75

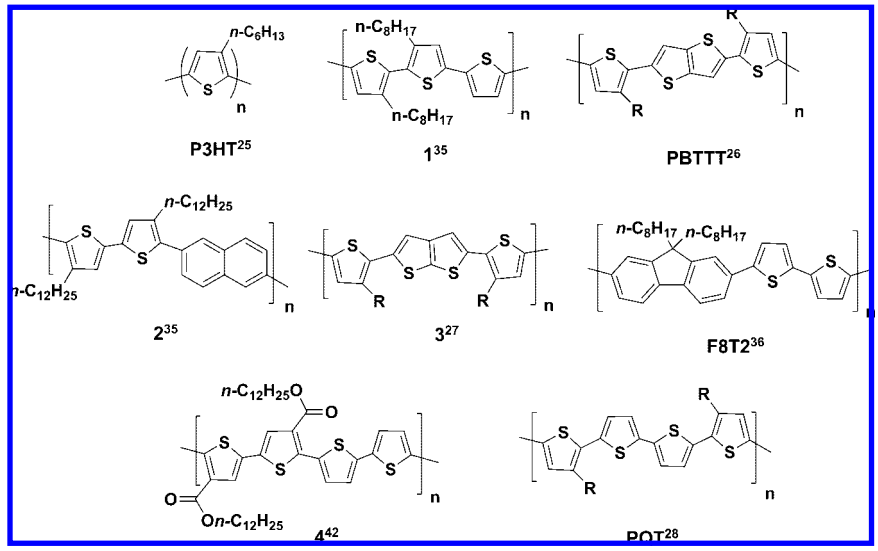

Figure 1. Structures of **P3HT** and air-stable thiophene-based polymeric semiconductors.

from solution,[19] presumably reflecting difficulties in creating high levels of long-range structural order. This lack of solution processibility, along with the intrinsic inefficiency of alternative vacuum vapor-phase film growth processes, limits the appeal of oligothiophenes as active channel materials in OTFTs.

For taking full advantage of the efficiencies of solution processing methodologies such as spin- coating,[20] stamping,[21] or inkjet printing,[22] polymeric organic semiconductors offer excellent candidate materials. Among the polythiophenes, soluble regioregular polythiophenes such as poly(3-hexylthiophene) (P3HT, Figure 1) and variants thereof[23–25] are among the most commonly used in OTFTs due to large charge carrier mobilities and synthetic accessibility.[26–29] Despite recent design advances, a major drawback of commonly used polythiophenes is poor air stability, a shortcoming that is particularly acute when these materials are used as the active layers in OTFTs. Unintentional doping of polythiophenes by ambient O_2 often results in large off-currents, leading to low current on/off ratios (I_{on}/I_{off}) and positive threshold voltage shifts.[23,30] Consequently, precautions must be taken during synthesis and device fabrication to exclude O_2.[31,32] These constraints thus render polythiophene-based OTFTs less attractive as cheap alternatives to silicon-based electronics. Thus, there is a continued need to develop semiconducting polymers with both high carrier mobility and air stability.

To a first approximation, the ambient air stability of organic semiconducting polymers toward oxidative doping is governed principally by the ionization potential[33]—or in terms of simple Koopmans' theorem[34] metrics, the energy of the highest-occupied molecular orbital (HOMO). Generally, increasing the ionization potential of organic semiconducting polymers improves environmental stability by minimizing the p-doping level achievable with ambient O_2. At the molecular level, the HOMO can be modified either by tailoring the effective conjugation length and/or by varying the electron density in the conjugated π-system. The effective conjugation length in polymers can be modulated by introducing rotational degrees of freedom, geometric twists, or less conjugated groups into the macromolecule backbone. For example, a polythiophene containing adjacent, twisted 3-octyl thiophene rings exhibits greater air stability than its regioregular head-to-tail counterpart (**1**, Figure 1).[35] Similarly, incorporation of either a thieno[3,2-*b*]thiophene (PBTTT, Figure 1), naphthalene (**2**, Figure 1), or thieno[2,3-*b*]thiophene unit (**3**, Figure 1) into the polymer backbone affords greater environmental stability,[26,27,35] and copolymers of thiophene with fluorene are reported to have good air stability and hole mobilities up to 0.01 $cm^2/V \cdot s - 0.02$ $cm^2/V \cdot s$ (F8T2, Figure 1).[36] An alternative approach to reducing the HOMO energy is to incorporate electron-withdrawing substituents. Reports of

(19) Katz, H. E.; Bao, Z. N.; Gilat, S. L. *Acc. Chem. Res.* **2001**, *34*, 359–369.
(20) Garnier, F.; Hajlaoui, R.; Yassar, A.; Srivastava, P. *Science* **1994**, *265*, 1684–1686.
(21) Rogers, J. A.; Bao, Z.; Baldwin, K.; Dodabalapur, A.; Crone, B.; Raju, V. R.; Kuck, V.; Katz, H.; Amundson, K.; Ewing, J.; Drzaic, P. *Proc. Natl. Acad. Sci. U.S.A.* **2001**, *98*, 4835–4840.
(22) Sirringhaus, H.; Kawase, T.; Friend, R. H.; Shimoda, T.; Inbasekaran, M.; Wu, W.; Woo, E. P. *Science* **2000**, *290*, 2123–2126.
(23) Bao, Z.; Dodabalapur, A.; Lovinger, A. J. *Appl. Phys. Lett.* **1996**, *69*, 4108–4110.
(24) Bao, Z. N.; Lovinger, A. J. *Chem. Mater.* **1999**, *11*, 2607–2612.
(25) Sirringhaus, H.; Brown, P. J.; Friend, R. H.; Nielsen, M. M.; Bechgaard, K.; Langeveld-Voss, B. M. W.; Spiering, A. J. H.; Janssen, R. A. J.; Meijer, E. W.; Herwig, P.; de Leeuw, D. M. *Nature* **1999**, *401*, 685–688.
(26) McCulloch, I.; Heeney, M.; Bailey, C.; Genevicius, K.; Macdonald, I.; Shkunov, M.; Sparrowe, D.; Tierney, S.; Wagner, R.; Zhang, W. M.; Chabinyc, M. L.; Kline, R. J.; Mcgehee, M. D.; Toney, M. F. *Nat. Mater.* **2006**, *5*, 328–333.
(27) Heeney, M.; Bailey, C.; Genevicius, K.; Shkunov, M.; Sparrowe, D.; Tierney, S.; McCulloch, I. *J. Am. Chem. Soc.* **2005**, *127*, 1078–1079.
(28) Ong, B. S.; Wu, Y. L.; Liu, P.; Gardner, S. *J. Am. Chem. Soc.* **2004**, *126*, 3378–3379.
(29) Pan, H.; Wu, Y.; Li, Y.; Liu, P.; Ong, B. S.; S.; Zhu, G. X. *Adv. Funct. Mater.* **2007**, *17*, 3574–3579.
(30) Meijer, E. J.; Detcheverry, C.; Baesjou, P. J.; van Veenendaal, E.; de Leeuw, D. M.; Klapwijk, T. M. *J. Appl. Phys.* **2003**, *93*, 4831–4835.
(31) Abdou, M. S. A.; Orfino, F. P.; Xie, Z. W.; Deen, M. J.; Holdcroft, S. *Adv. Mater.* **1994**, *6*, 838–841.
(32) Ficker, J.; Ullmann, A.; Fix, W.; Rost, H.; Clemens, W. *J. Appl. Phys.* **2003**, *94*, 2638–2641.
(33) de Leeuw, D. M.; Simenon, M. M. J.; Brown, A. R.; Einerhand, R. E. F. *Synth. Met.* **1997**, *87*, 53–59.
(34) Koopmans, T. *Physica* **1933**, *1*, 104.
(35) McCulloch, I.; Bailey, C.; Giles, M.; Heeney, M.; Love, I.; Shkunov, M.; Sparrowe, D.; Tierney, S. *Chem. Mater.* **2005**, *17*, 1381–1385.

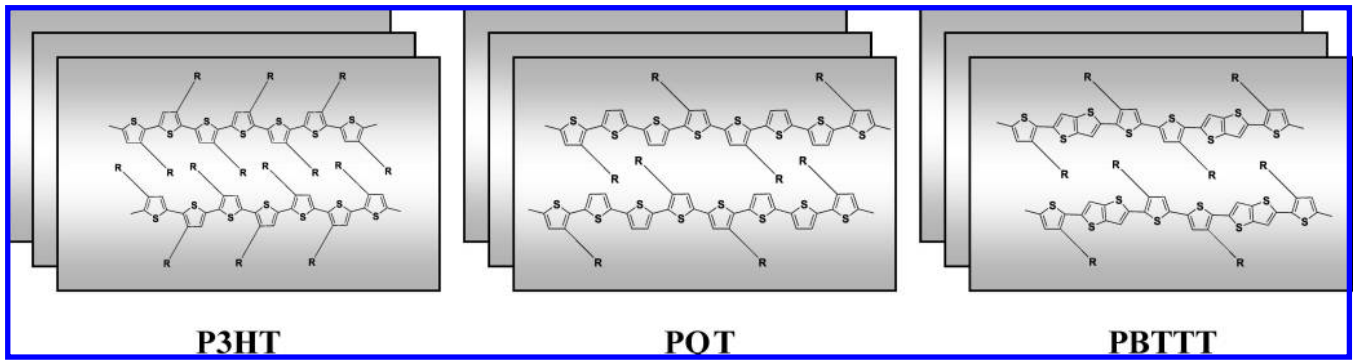

Figure 2. Schematic of the lamellar π-stacking in polymers **P3HT**, **PQT**, and **PBTTT**.

polythiophenes with electron-withdrawing substituents are rare, doubtless due to synthetic challenges.[37,38] For example, polythiophenes bearing carboxylate groups at the 3-position have been synthesized using Ullmann,[39,40] Kumada,[41] and Stille coupling reactions[42] (e.g., **4**, Figure 1). These polymers exhibit increased oxidation potentials due to the presence of the electron-withdrawing substituents; as a result, OTFT devices based on these polymers are reported to exhibit air stability superior to that of P3HT-based devices.[42] PBTTT[26] and PQT[28] also exhibit enhanced FET performance with good ambient stabilities due to their highly organized film microstructures and larger ionization potentials in comparison to P3HT; highly ordered, lamellar π-stacks of these polymers are oriented normal to the substrate and lead to high OTFT mobilities (Figure 2).[43–45]

Silicon substituents are known to stabilize adjacent carbanionic centers due to the effective hyperconjugation between negatively charged carbon centers and the adjacent silyl groups.[46] Among the various silicon-containing π-conjugated systems, silole (sila-2,4-cyclopentadiene, Figure 3)-containing polymers have attracted recent attention as novel systems in which the exocyclic Si−C σ*-orbital effectively mixes with the π*-orbital of the butadiene fragment to afford a low-lying lowest-unoccupied molecular orbital (LUMO) and a relatively small band gap.[47–49] Additionally, silicon introduction stabilizes the diene HOMO level compared to the carbon counterparts,[48]

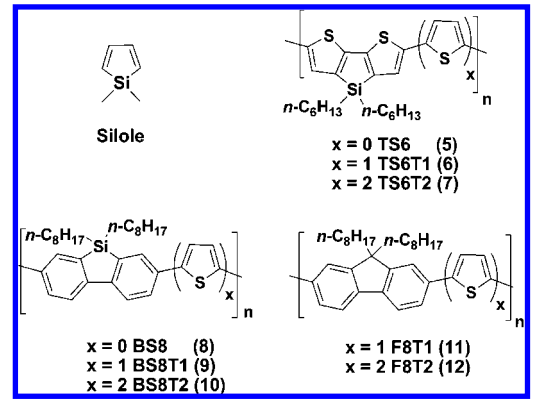

Figure 3. Structures of silole−thiophene polymers **5**−**10** and fluorene−thiophene polymers **11** and **12**.

which should, *a priori*, enhance the ambient stability of silole-polymer-derived TFTs. To date, however, the use of polymeric silole derivatives has been limited to electron-transporting materials in OLEDs[50–54] and solar cells.[55,56] Only recently have silole-containing polymers been investigated as the active layer in OTFTs.[57–59] Nevertheless, the performance of the reported materials is generally modest in regard to carrier mobility and I_{on}/I_{off}, probably because nonbonded repulsions between the large substituents at the silole 3- and 4-positions interfere with the close $\pi-\pi$ stacking requisite for efficient charge transport.[60]

In a recent communication,[61] we briefly described the synthesis and characterization of several solution-processible silole-containing polythiophenes (**6**, **7**, **9**, **10**; Figure 3). Preliminary electrical measurements revealed the curious result *that each of these new polymers is a p-channel semiconductor* and,

(36) Sirringhaus, H.; Wilson, R. J.; Friend, R. H.; Inbasekaran, M.; Wu, W.; Woo, E. P.; Grell, M.; Bradley, D. D. C. *Appl. Phys. Lett.* **2000**, *77*, 406–408.
(37) Masuda, H.; Kaeriyama, K. *Makromol. Chem., Rapid Commun.* **1992**, *13*, 461–465.
(38) Waltman, R. J.; Diaz, A. F.; Bargon, J. *J. Electrochem. Soc.* **1984**, *131*, 1452–1456.
(39) Pomerantz, M.; Yang, H.; Cheng, Y. *Macromolecules* **1995**, *28*, 5706–5708.
(40) Pomerantz, M.; Cheng, Y.; Kasim, R. K.; Elsenbaumer, R. L. *J. Mater. Chem.* **1999**, *9*, 2155–2163.
(41) Amarasekara, A. S.; Pomerantz, M. *Synthesis* **2003**, 2255–2258.
(42) Murphy, A. R.; Liu, J. S.; Luscombe, C.; Kavulak, D.; Frechet, J. M. J.; Kline, R. J.; McGehee, M. D. *Chem. Mater.* **2005**, *17*, 4892–4899.
(43) Chabinyc, M. L.; Toney, M. F.; Kline, R. J.; McCulloch, I.; Heeney, M. *J. Am. Chem. Soc.* **2007**, *129*, 3226–3237.
(44) Kline, R. J.; DeLongchamp, D. M.; Fischer, D. A.; Lin, E. K.; Richter, L. J.; Chabinyc, M. L.; Toney, M. F.; Heeney, M.; McCulloch, I. *Macromolecules* **2007**, *40*, 7960–7965.
(45) DeLongchamp, D. M.; Kline, R. J.; Lin, E. K.; Fischer, D. A.; Richter, L. J.; Lucas, L. A.; Heeney, M.; McCulloch, I.; Northrup, J. E. *Adv. Mater.* **2007**, *19*, 833–837.
(46) Wetzel, D. M.; Brauman, J. I. *J. Am. Chem. Soc.* **1988**, *110*, 8333–8336.
(47) Risko, C.; Kushto, G. P.; Kafafi, Z. H.; Bredas, J. L. *J. Chem. Phys.* **2004**, *121*, 9031–9038.
(48) Yamaguchi, S.; Tamao, K. *Bull. Chem. Soc. Jpn.* **1996**, *69*, 2327–2334.
(49) Zhan, X. W.; Risko, C.; Amy, F.; Chan, C.; Zhao, W.; Barlow, S.; Kahn, A.; Bredas, J. L.; Marder, S. R. *J. Am. Chem. Soc.* **2005**, *127*, 9021–9029.
(50) Chan, K. L.; McKiernan, M. J.; Towns, C. R.; Holmes, A. B. *J. Am. Chem. Soc.* **2005**, *127*, 7662–7663.
(51) Chen, J. W.; Law, C. C. W.; Lam, J. W. Y.; Dong, Y. P.; Lo, S. M. F.; Williams, I. D.; Zhu, D. B.; Tang, B. Z. *Chem. Mater.* **2003**, *15*, 1535–1546.
(52) Liu, M. S.; Luo, J. D.; Jen, A. K. Y. *Chem. Mater.* **2003**, *15*, 3496–3500.
(53) Murata, H.; Kafafi, Z. H.; Uchida, M. *Appl. Phys. Lett.* **2002**, *80*, 189–191.
(54) Tamao, K.; Uchida, M.; Izumizawa, T.; Furukawa, K.; Yamaguchi, S. *J. Am. Chem. Soc.* **1996**, *118*, 11974–11975.
(55) Mi, B. X.; Dong, Y. Q.; Li, Z.; Lam, J. W. Y.; Haussler, M.; Sung, H. H. Y.; Kwok, H. S.; Dong, Y. P.; Williams, I. D.; Liu, Y. Q.; Luo, Y.; Shuai, Z. G.; Zhu, D. B.; Tang, B. Z. *Chem. Commun.* **2005**, 3583–3585.
(56) Boudreault, P.-L. T.; Michaud, A.; Leclerc, M. *Macromol. Rapid Commun.* **2007**, *28*, 2176–2179.

Scheme 1. Synthesis of Dibenzosilole and Dithienosilole Monomers

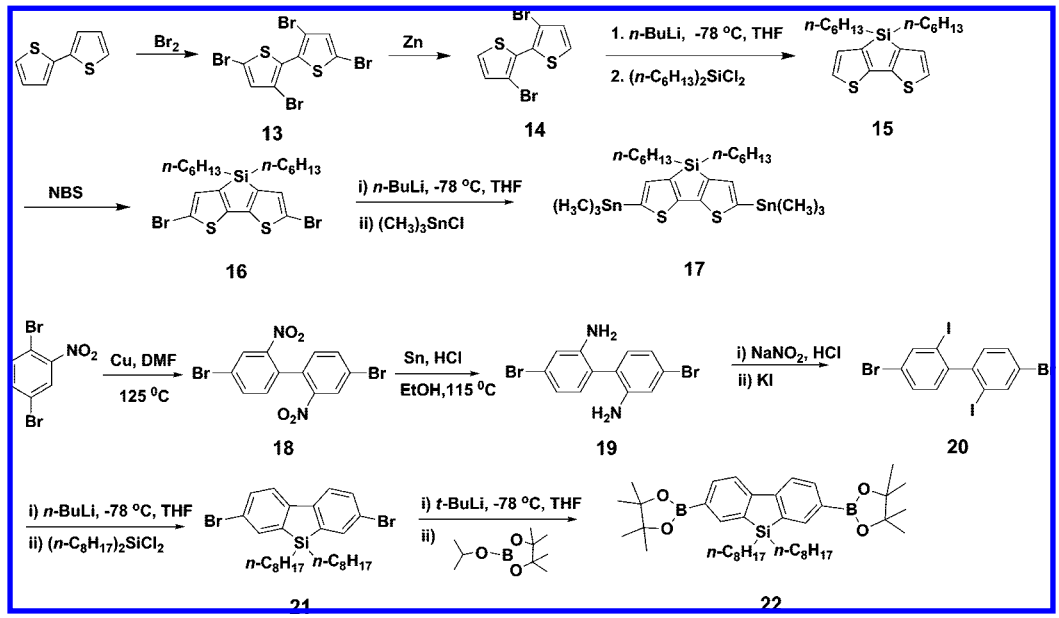

despite the depressed LUMO energies, exhibit no evidence of n-channel transport. We also provided preliminary evidence that these polythiophenes exhibit good air and thermal stability. The silole-containing polythiophenes were found to exhibit useful FET properties after thermal annealing, and the devices appeared to be stable to air without protective encapsulation. In this contribution, we report in full on the synthesis and characterization of two new silole-based polymers, **5** and **8**, to further explore and elucidate architecture-electronic structure relationships in a series of silole-based polymers, and their impact on OTFT performance. New synthetic routes to polymers **5**−**10** are also explored to enhance the molecular weight and processing characteristics. TFT devices based on polymers **5**−**10** have been optimized in terms of solvent selection and film processing methodology. It will be seen that materials having hole mobilities approaching 0.1 $cm^2/V \cdot s$ with $I_{on}/I_{off} > 10^6$ can now be obtained with devices fabricated in ambient atmosphere using simple spin-coating techniques. Furthermore, the first example of TFT fabrication with a gravure-printed semiconductor on a gravure-printed dielectric is reported. Finally, the silole polymer electronic structures are analyzed in depth using density functional theory (DFT). The result is a detailed description of the electronic structures of polymers **5**−**10** that, when combined with the experimental characterization data, provides clear insight into the OTFT performance and reveals the basis of the previously enigmatic hole-transporting characteristics. Two new fluorene-containing copolymers, **11** and **12** (F8T2), are also synthesized and fully characterized. TFTs based on **11**, **12**, and **P3HT** are fabricated and evaluated for comparative purposes.

Results

Synthesis. As shown in Scheme 1, dibromo-functionalized dithienosilole- and dibenzosilole-based building blocks **16** and **21** were prepared from commercially available bithiophene and 2,5-dibromonitrobenzene, respectively. To synthesize polymers **5**−**12**, Suzuki and Stille coupling polymerization reactions were conducted as shown in Scheme 2. The building block 3,3′-di-*n*-hexylsilylene-2,2′-bithiophene (**15**) was prepared via a reported procedure[62] in which bithiophene is first brominated to give 3,5,3′,5′-tetrabromobithiophene (**13**) that is then selectively debrominated with Zn to give 3,3′-dibromobithiophene (**14**). Double lithiation of **14** with *n*-butyllithium followed by subsequent cyclization with di-*n*-hexyldichlorosilane yields dithienosilole monomer **15**. Dibromo-functionalized monomer **16** is then prepared by bromination with NBS in DMF. The overall yield for monomer **16** is 43%. Dithienosilole monomer **16** is transformed into distannyl reagent **17** by treatment of **16** with *n*-BuLi followed by trimethyltin chloride. Building block 2,7-dibromo-9,9-dioctyldibenzosilole (**21**) is prepared by a known procedure.[50] Ullmann coupling product **18** is reduced to the corresponding diamine **19**, and Sandmeyer reaction of **19** with sodium nitrite in concentrated HCl, followed by the addition of a 10-fold excess of concentrated KI solution, gives biphenyl **20** in 28% yield. Conventional Sandmeyer reactions with stoichiometric amounts of KI result in lower yields of 10%−15% for **20**. The low yield is presumably the result of intramolecular cyclization of the initial monoiodo-substituted product via attack of the iodo substituent on the neighboring 2′-position with decomposition of the second diazonium substituent to give dibenzoiodonium iodide.[63] Selective translithiation of the 2,2′-iodo-substituents of **20** with *n*-BuLi in THF followed by subsequent cyclization with di-*n*-octyldichlorosilane affords dibenzosilole monomer **21**. The overall yield for monomer **21** is 16%. Since pinacolato boronic esters are reported to be significantly more stable than boronic acids and are frequently used in Suzuki coupling reactions to prepare biaryl

(57) Wang, Y.; Hou, L. T.; Yang, K. X.; Chen, J. W.; Wang, F.; Cao, Y. *Macromol. Chem. Phys.* **2005**, *206*, 2190–2198.
(58) Ohshita, J.; Lee, K. H.; Hamamoto, D.; Kunugi, Y.; Ikadai, J.; Kwak, Y. W.; Kunai, A. *Chem. Lett.* **2004**, *33*, 892–893.
(59) Wang, F.; Luo, J.; Yang, K. X.; Chen, J. W.; Huang, F.; Cao, Y. *Macromolecules* **2005**, *38*, 2253–2260.
(60) Hutchison, G. R.; Ratner, M. A.; Marks, T. J. *J. Am. Chem. Soc.* **2005**, *127*, 16866–16881.
(61) Usta, H.; Lu, G.; Facchetti, A.; Marks, T. J. *J. Am. Chem. Soc.* **2006**, *128*, 9034–9035.
(62) Chen, W. PhD Thesis, Iowa State University, 1997.
(63) Lothrop, W. C. *J. Am. Chem. Soc.* **1941**, *63*, 1187–1191.

Scheme 2. Synthesis of Dibenzosilole-Based and Dithienosilole-Based Homo- and Copolymers

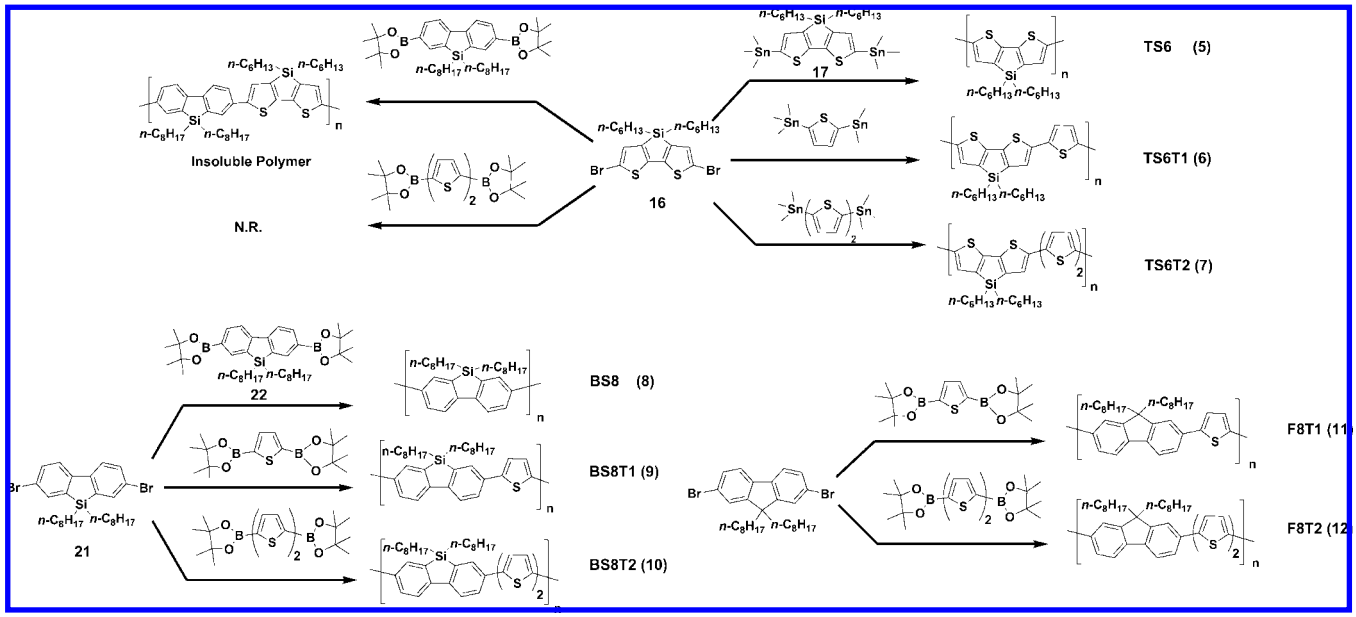

Table 1. Physicochemical Properties [Molecular Weight (M_w, KD), Polydispersity (PD), Melting Temperature (T_m), Crystallization Temperature (T_c), Onset Decomposition Temperature (T_d), Solution (in THF) and Film Optical Absorption Maxima, Emission Maxima (in THF) (λ, nm), Energy Gaps ($E_{g,op}$, eV)] and FET Performance Summary (OFET Charge Carrier Mobilities (μ, $cm^2\ V^{-1}\ s^{-1}$) and Current On/Off Ratios (I_{on}/I_{off}) in Air) of Polymers **5**−**12**

polymer	polymerization protocol	M_w (PD) (KD)	T_m, T_c[a] (°C)	T_d[c] (°C)	λ_{sol} ($E_{g,op}$)[d] (nm, eV)	λ_{film} ($E_{g,op}$)[d] (nm, eV)	λ_{em} (nm)	FET μ_h (cm^2/V s)	FET I_{on}/I_{off}
TS6 (**5**)	Stille	26 (2.9)	-[b]	250	533 (1.9)	535 (1.8)	601	-[b]	-[b]
TS6T1 (**6**)	Stille	30 (2.9)	257, 230	480	521 (2.0)	574 (1.8)	611	0.05	1×10^5
TS6T2 (**7**)	Stille	41 (3.0)	300, -[b]	445	544 (1.9)	545 (1.9)	620	0.08	5×10^4
BS8 (**8**)	Suzuki	32 (3.4)	-[b]	410	377 (3.0)	401 (2.9)	455	-[b]	-[b]
BS8T1 (**9**)	Suzuki	112 (3.1)	253, -[b]	420	471 (2.5)	484 (2.5)	488	6×10^{-5}	3×10^4
BS8T2 (**10**)	Suzuki	127 (3.7)	340, 295	430	503 (2.3)	493 (2.3)	528	0.006	4×10^6
F8T1 (**11**)	Suzuki	17 (2.6)	267, -[b]	415	427 (2.6)	440 (2.5)	469	9×10^{-5}	2×10^5
F8T2 (**12**)	Suzuki	80 (3.3)	259 and 277, 196	425	456 (2.4)	460 (2.4)	496	0.006	2×10^5

[a] Melting temperature (T_m) and crystallization temperature (T_c) determined by DSC. [b] Not observed. [c] Onset decomposition temperature measured by TGA under nitrogen. [d] Optical band gap estimated from the low energy band edge in the optical spectrum.

compounds and polymers,[64,65] compound **21** was converted to pinacolato ester **22** by treatment with *t*-BuLi, followed by 4,4,5,5-tetramethyl-[1,3,2]dioxaborolane, for use as the comonomer in the homopolymerization with monomer **21**.

Polymers **5**−**12** were synthesized according to Scheme 2. Dithienosilole-based polymers **5**−**7** were synthesized via a Stille polycondensation between reagents **16** and **17**, 2,5-bis(trimethylstannyl)thiophene, and 2,5′- bis(trimethylstannyl)bithiophene, respectively, in good yields (see Supporting Information). Dibenzosilole-based polymers **8**−**10** were prepared via a Suzuki polycondensation protocol between reagents **21** and **22**, 2,5-bis(4,4,5,5-tetramethyl-1,3,2-dioxaborolan-2-yl)thiophene, and 2,5′-bis(4,4,5,5-tetramethyl-1,3,2-dioxaborolan-2-yl)bithiophene, respectively, in moderate to good yields (See Supporting Information). The syntheses of the fluorene-thiophene copolymers **11** and **12** were performed by reported procedures.[66,67] The physicochemical properties of polymers **5**−**12** are summarized in Table 1. The molecular weights (M_w's) of **5**−**7** determined by high-temperature GPC were 26 KD (PDI = 2.9), 30 KD (PDI = 2.9), and 41 KD (PDI = 3.0), respectively. These macromolecules are freely soluble in common nonprotic organic solvents such as THF, toluene, xylenes, chloroform, methylene chloride, chlorobenzene, *o*-dichlorobenzene (DCB), and 1,2,4-trichlorobenzene (TCB). GPC-derived molecular weights (M_w) of the dibenzosilole-based polymers **8**−**10** are 32 KD (PDI = 3.4), 112 KD (PDI = 3.1), and 127 KD (PDI = 3.7), respectively. Polymer **8** is very soluble in common nonprotic organic solvents, but the solubilities of **9** and **10** are lower than dithienosilole-based polymers **5**−**7.** They are only soluble in chlorinated aromatic solvents such as warm chlorobenzene, DCB, and TCB; this is probably a consequence of the higher molecular weights of **9** and **10**. Fluorene-based copolymers **11** and **12** have GPC-derived molecular weights of 17 KD (PDI = 2.6) and 80 KD (PDI = 3.3), respectively. They are soluble in hot toluene, xylene, and chlorobenzene. Each of the new polymers was fully characterized by ^1H and ^{13}C NMR (features are broad as expected), optical spectroscopy, PL, GPC, TGA, DSC, and elemental analysis. Details are given in the Supporting Information.

(64) Murata, M.; Oyama, T.; Watanabe, S.; Masuda, Y. *J. Org. Chem.* **2000**, *65*, 164–168.
(65) Ishiyama, T.; Murata, M.; Miyaura, N. *J. Org. Chem.* **1995**, *60*, 7508–7510.
(66) Bernius, M.; Inbasekaran, M.; Woo, E.; Wu, W. S.; Wujkowski, L. *J. Mater. Sci.: Mater. Electron.* **2000**, *11*, 111–116.
(67) Inbasekaran, M.; Wu, W.; Woo, E. P. Process for preparing conjugated polymers. U.S. Patent 5,777,070, 1998.

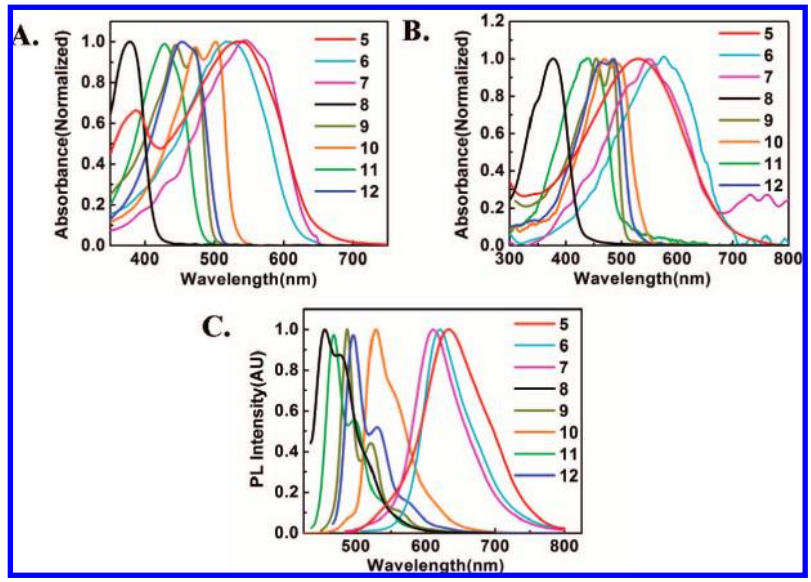

Figure 4. UV−vis absorption spectra of polymers **5**−**12** in THF solution (A), as thin films on glass substrates (B), and photoluminescence spectra in THF solution (C).

In order to optimize the molecular weights of polymers **5**−**7**, a Suzuki polycondensation protocol was investigated. However, all attempts under typical Suzuki polymerization conditions produced low-molecular weight oligomers, and negligible polymeric products were obtained. This is presumably due to deboronation side reactions that occur prior to aryl−aryl coupling, thus limiting formation of the desired products. These types of side reactions are well-documented.[35,68–73] In contrast, thiophene−phenylene copolymers with satisfactory molecular weights have previously been synthesized using Suzuki polycondensation,[69,74,75] consistent with the present syntheses of dibenzosilole−thiophene copolymers. A copolymer containing dithienosilole and dibenzosilole units was also synthesized via Suzuki polycondensation (Scheme 2). However, the polymer was not soluble in the aforementioned solvents, hindering further purification, characterization, and device fabrication. Halting the polymerization processes at the early stages of reaction (reducing the reaction time), in the hope of obtaining lower molecular weight polymers, yielded no soluble polymeric products. In order to observe the effects of end-capping processes on the physicochemical properties and FET performances of the target polymers, reactions with end-capping reagents such as bromobenzene, benzeneboronic acid pinacol ester, 2-bromothiophene, and 2-tributylstannyllthiophene were performed on the highest mobility polymers of each polymer series (compounds **7** and **10**). However, the purified polymers exhibit no differences in electronic/device properties, consistent with the reported semiconducting polymers prepared without endcapping reagents.[26,27,35,42] Eventually, we decided to avoid the additional end-capping steps and therefore report experimental procedures here without the end-capping steps.

Thermal Properties. Thermogravimetric analysis (TGA, heating ramp rate of 10 °C/min under N_2) was used to determine the thermal stability of polymers **5**−**12** (Figure S1). A 5% mass loss is defined as the thermolysis threshold. The thermolysis onset temperature for polymer **5** is ∼250 °C, while polymers **6**−**12** all have onset temperatures above 400 °C, indicative of good thermal stability.

The thermal properties of the present polymers were also examined by differential scanning calorimetry (DSC) at a scanning speed of 10 °C/min (Figure S2). Polymer **6** exhibits a single endotherm/exotherm at ∼250 °C on heating/cooling, while **7** exhibits one broad endotherm near 300 °C. For both polymers, the endotherms and exotherms are reversible over many cycles. Polymer **9** exhibits a broad transition at 253 °C in the heating cycle, and an exotherm is not observed in the cooling cycle; similar observations are made for polymer **11**, which exhibits a single endotherm at ∼267 °C. For polymer **10**, there is an endothermic melting feature at 340 °C in the heating cycle that is tentatively attributed to backbone melting. Upon cooling, an exothermic recrystallization peak is observed at 295 °C. Both the melting and recrystallization peaks are completely reversible over four cycles. The DSC of polymer **12** exhibits two endotherms at 259 and 277 °C and one exotherm at 196 °C upon cooling, consistent with a previous report.[76]

On average, the polymers containing bithiophene units have higher melting temperatures, suggesting closer packing in the solid state. The melting temperatures of pair **6** and **9** and pair **7** and **10** are rather comparable. Silicon substitution lowers the T_m for **9** by ∼15 °C compared to **11** but increases the T_m and T_c of **10** by 60−100 °C compared to polymer **12**.

Optical Properties. Solution and thin-film UV−vis absorption spectra for polymers **5**−**12** are shown in Figure 4A and B, and data are collected in Table 1. Note that the differences in the optical properties of these polymers reflect the differences in

(68) Jayakannan, M.; van Dongen, J. L. J.; Janssen, R. A. J. *Macromolecules* **2001**, *34*, 5386–5393.
(69) Forster, M.; Annan, K. O.; Scherf, U. *Macromolecules* **1999**, *32*, 3159–3162.
(70) Gronowitz, S.; Bobosik, V.; Lawitz, K. *Chem. Scr.* **1984**, *23*, 120–122.
(71) Gronowitz, S.; Lawitz, K. *Chem. Scr.* **1983**, *22*, 265–266.
(72) Kirschbaum, T.; Azumi, R.; Mena-Osteritz, E.; Bauerle, P. *New J. Chem.* **1999**, *23*, 241–250.
(73) Kirschbaum, T.; Briehn, C. A.; Bauerle, P. *J. Chem. Soc., Perkin Trans. 1* **2000**, *8*, 1211–1216.
(74) Kaeriyama, K.; Tsukahara, Y.; Negoro, S.; Tanigaki, N.; Masuda, H. *Synth. Met.* **1997**, *84*, 263–264.
(75) Shin, S. H.; Park, J. S.; Park, J. W.; Kim, H. K. *Synth. Met.* **1999**, *102*, 1060–1062.
(76) Brennan, D. J.; Townsend, P. H.; Welsh, D. M.; Dibbs, M. G.; Shaw, J. M.; Miklovich, J. L.; Boeke, R. B. *Mater. Res. Soc. Symp. Proc.* **2003**, *771*, L6.1.1L6.1.5.

the chemical structures since the number-average degrees of polymerization (DPs) are sufficiently large (>15) to make contributions of the molecular weights negligible.[17,77,78] In THF, polymer **5** exhibits a single absorption maximum at 533 nm, while the solution-cast thin film, which is discontinuous on glass substrates, shows a similar absorption maximum at 535 nm. The absorption maxima for **6** and **7** are located at 521 and 544 nm, respectively, in THF. Polymers **6** and **7** form smooth and shiny thin films when solutions are cast on silicon wafers and exhibit absorption maxima at 574 nm for polymer **6** and at 545 nm for polymer **7**. Polymers **5** and **7** exhibit little difference in absorption maxima upon going from the solution to thin film phase; however, the absorption maximum red-shifts ~50 nm for polymer **6** in the thin film vs solution, suggesting a high degree of macromolecular organization in the thin film phase.

The optical absorption spectra of dibenzosilole-based polymers **8**−**10** have absorption maxima that are blue-shifted compared to those of dithienosilole-based polymers **5**−**7**. The absorption maximum for homopolymer **8** occurs at 377 nm, corresponding to the largest $\pi-\pi^*$ transition energy in the silole-based polymer series. Polymers **9** and **10** exhibit two absorption maxima located at 444 and 471 nm for **9** and 473 and 503 nm for **10**. These transitions likely correspond to predominantly local transitions of the constituent dibenzosilole and mono/bithiophene copolymer building blocks. The absorption maxima of polymers **8**−**10** cast as thin films are at 401 nm (**8**), 484 nm (**9**), and 493 nm (**10**). The fluorene-based copolymers exhibit maxima at 427 nm in solution and 440 nm as a thin film for **11** and 456 nm in solution (with a strong shoulder at 502 nm) and 460 nm as a thin film for **12**. Dibenzosilole-based copolymers **9** and **10** exhibit significant bathochromic shifts of *ca*. 30−50 nm compared to the fluorene-based polymers **11** and **12**. In both cases, annealing has little impact on the film absorption maxima. Additionally, on proceeding from **8** to **5**, **9** to **6**, and **10** to **7**, the large bathochromic shifts (40−60 nm in THF, 50−130 nm in thin film) in the absorption maximum trends reflect effects from both the π-electron-donating S atom vs the −C≡C− linkage and the more planar conformation of five−five vs five−six inter-ring linkages.

Band gaps for the present polymer series are estimated from the low-energy band edges of the thin-film optical spectra, taking 10% of the maximum as the band edge (see Table 1). The optical band gaps of polymers **5**, **6**, and **7** are estimated to be 1.8, 1.8, and 1.9 eV, respectively, and are similar to that of P3HT (1.9 eV).[79] These small band gaps likely reflect the appreciable planarity of these macromolecules (*vide infra*) and the backbone similarity to polythiophenes. Larger band gaps are observed for the dibenzosilole-based polymers vs dithienosilole-based polymers; the optical band gaps of polymers **8**, **9**, and **10** are estimated to be 2.9, 2.5, and 2.3 eV, respectively. The optical band gaps for materials **11** and **12** are estimated to be 2.5 and 2.4 eV, respectively. Similarities in the optical band gaps of pair **10** and **12** and pair **9** and **11** suggest similarly extended π-conjugation.

The solution PL emission spectra are shown in Figure 4C and data collected in Table 1. The dithienosilole-based polymers emit orange-red light with maxima at 601, 611, and 620 nm for **5**, **6**, and **7**, respectively. The dibenzosilole-based polymers exhibit well-resolved vibronic structures for the shorter-wavelength emission maxima. While homopolymer **8** emits blue light with a maximum at 455 nm, copolymers **9** and **10** show green-yellow emission with maxima at 488 and 528 nm, respectively; these transitions are assigned to the 0−0 transition in dilute solutions. The 0−1 and 0−2 transitions in the PL emission spectra are observed at 477 and 512 nm for **8** and at 521 and 561 nm for **9**. Polymer **10** exhibits a 0−1 transition at 555 nm. The 100−150 nm red-shift of emission maxima for **5**−**7** vs the dibenzosilole-based polymers **8**−**10** likely indicates weaker π-conjugation in the latter systems. Fluorene-based polymers **11** and **12** exhibit hypsochromic shifts vs the dibenzosilole-based polymers with emission maxima at 469 and 496 nm, respectively. Polymers **9** and **10** exhibit emissions which are ~20−30 nm red-shifted compared to those of fluorene-based polymers **11** and **12**. The dithienosilole-based polymers **5**−**7** and homopolymer **8** exhibit large Stokes' shifts of ~70−90 nm, which are not unusual for silicon-containing polymers,[80] and may possibly be due to excimer emission.[81,82] Polymers **9** and **10** exhibit modest Stokes shifts of ~20 nm between the absorption and emission maxima, which are smaller than those of polymers **11** and **12** (~40 nm); this suggests a greater rigidity in the dibenzosilole-based polymers.

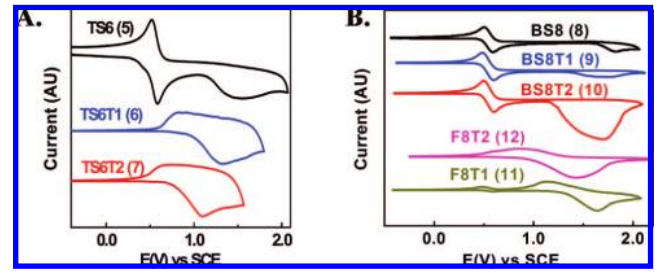

Figure 5. Cyclic voltammograms of polymers **5**−**12** as thin films in 0.1 M $Bu_4N^+PF_6^-$ solution in acetonitrile at a scan rate of 100 mV/s. In all experiments, ferrocene is used as the internal standard.

Table 2. Electrochemical Properties of Polymers **5**−**12**

polymer	E_{ox}^{onset} (V)[a]	E_{ox}^{f} (V)[b]	HOMO^{ox} (eV)[c]	$E_{g,op}$ (eV)[c]	LUMO^{ox} (eV)[c]
TS6 (**5**)	1.2	1.5	−5.6	1.8	−3.8
TS6T1 (**6**)	0.9	1.3	−5.3	1.8	−3.5
TS6T2 (**7**)	0.8	1.1	−5.2	1.9	−3.3
BS8 (**8**)	1.6	1.8	−6.0	2.9	−3.1
BS8T1 (**9**)	1.4	1.8	−5.8	2.5	−3.3
BS8T2 (**10**)	1.2	1.7	−5.6	2.3	−3.3
F8T1 (**11**)	1.3	1.6	−5.7	2.5	−3.2
F8T2 (**12**)	1.0	1.4	−5.4	2.4	−3.0

[a] Onset voltage for oxidation vs SCE. [b] Formal oxidation potential. [c] HOMO^{ox} ≡ IP^{ox} and LUMO^{ox} ≡ HOMO + $E_{g,op}$; see eq 1.

Electrochemical Properties. Oxidation and reduction potentials for the present polymer series were obtained using cyclic voltammetry (CV). Cyclic voltammograms of the polymer thin films are shown in Figure 5, and electrochemical data are summarized in Table 2. The dithienosilole-based polymers **5**, **6**, and **7** exhibit oxidation onset potentials of 1.2, 0.9, and 0.8 V, respectively (vs SCE), with formal oxidation potentials in the range 1.1−1.5 V (vs SCE). The onset oxidation potentials

(77) Hutchison, G. R.; Ratner, M. A.; Marks, T. J. *J. Phys. Chem. A* **2002**, *106*, 10596–10605.
(78) Hutchison, G. R.; Ratner, M. A.; Marks, T. J. *J. Phys. Chem. B* **2005**, *109*, 3126–3138.
(79) Chen, T. A.; Wu, X. M.; Rieke, R. D. *J. Am. Chem. Soc.* **1995**, *117*, 233–244.
(80) Wang, W.-Y.; Wang, C.-K.; Poon, S.-Y.; Lee, A. W.-M.; Tian, M.; Xin, W. *Macromol. Rapid Commun.* **2005**, *26*, 376–380.
(81) Jenekhe, S. A.; Osaheni, J. A. *Science* **1994**, *265*, 765–768.
(82) Prieto, I.; Teetsov, J.; Fox, M. A.; Vanden Bout, D. A.; Bard, A. J. *J. Phys. Chem. A* **2001**, *105*, 520–523.

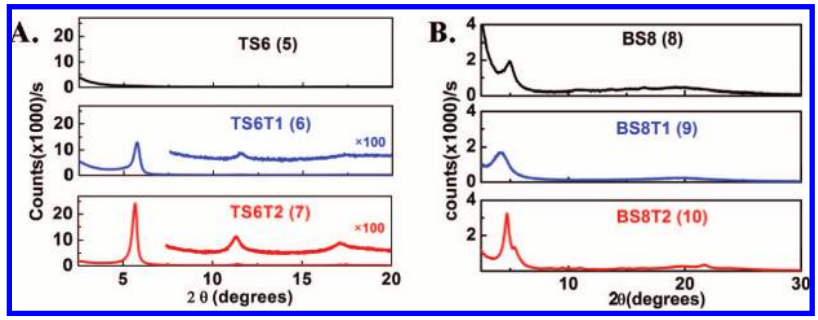

Figure 6. $\theta-2\theta$ X-ray diffraction (XRD) scans of drop-cast films of polymers **5**−**10** on silicon substrates.

for the dibenzosilole-based polymers are 1.6, 1.4, and 1.2 V (vs SCE) for **8**, **9**, and **10**, respectively, which are ∼0.4−0.5 V greater than those for the dithienosilole-based polymers, and suggest higher stability with respect to oxidative doping. The formal oxidation potentials for **8**−**10** are determined to be in the range 1.7−1.8 V (vs SCE). Electrochemical characterization of the fluorene-based copolymers gives onset and formal oxidation potentials of 1.3 and 1.6 V, respectively, for **11**, and 1.0 and 1.4 V, respectively, for **12**. None of these polymers exhibit obvious reduction peaks, suggesting that they are intrinsically more suitable for p-type charge conduction vs n-type conduction.[83]

From these oxidation potentials, the ionization potentials ($IP^{ox} \approx -HOMO^{ox}$, assuming that Koopmans' theorem holds) for the present polymers can be estimated by taking the SCE energy level to be −4.4 eV below the vacuum level and using the relation of eq 1.[84]

$$HOMO^{ox} = -E_{ox\text{-}onset} - 4.4 \quad (1)$$

Using this relationship, the $HOMO^{ox}$ values for the dithienosilole-based polymers are estimated to lie at −5.6, −5.3, and −5.2 eV for **5**, **6**, and **7**, respectively, indicative of larger ionization energies vs P3HT (∼ −4.9 eV).[85] The introduction of the silole core into the thiophene backbone thus stabilizes the system with respect to ionization with no significant compromise of the effective π-conjugation vs P3HT, as observed in the similar optical band gaps (*vide supra*). The solid state $HOMO^{ox}$'s of the dibenzosilole-based polymers are similarly estimated to lie at −6.0, −5.8, and −5.6 eV for polymers **8**, **9**, and **10**, respectively, suggesting that introduction of the electron-deficient dibenzosilole unit into the thiophene backbone dramatically depresses the HOMO level. For comparison, electrochemical characterization of fluorene-based copolymers **11** and **12** gives $HOMO^{ox}$ energies of −5.7 and −5.4 eV, respectively. Dibenzosilole−thiophene copolymers **9** and **10** have electrochemically estimated ionization energies ∼0.1−0.2 eV greater than those of the analogous carbon versions of the same polymers, **11** and **12**, in agreement with the effects deduced from electronic structure calculations (*vide infra*).[86–88] The electrochemical measurements suggest marked destabilization of the HOMO levels and lesser stabilization of the LUMO levels on proceeding from the fused biphenylene rings of fluorene and dibenzosilole to the fused bithiophene ring of dithienosilole.[89]

X-ray Diffraction (XRD) Analysis. Microstructural order in the silole-based homo- and copolymer thin films was assayed by $\theta-2\theta$ X-ray diffraction (XRD) scans (Figure 6). The measurements were taken on drop-cast films prepared from 0.5 wt % solutions in THF or 1,2,4-trichlorobenzene and annealed at 250 °C under nitrogen for 30 min. The thickness of the films was determined to be 250−300 nm by profilometry. As shown in Figure 6, each polymer thin film, with the exception of dithienosilole homopolymer **5**, is crystalline. Polymers **6** and **7** exhibit highly crystalline patterns with diffraction peaks up to third-order, indicating a high degree of solid state ordering. Distinct primary diffraction features are observed at $2\theta = 5.68°$ and 5.74°, corresponding to *d*-spacings of 15.54 and 15.38 Å for polymers **6** and **7**, respectively. Dibenzosilole-based polymers **8**−**10** exhibit substantially broader or weaker diffraction features compared to **6** and **7**. Homopolymer **8** has a single major reflection at $2\theta = 4.97°$, corresponding to a *d*-spacing of 17.76 Å. Polymers **9** and **10** have single major reflections at $2\theta = 4.22°$ and 4.72°, corresponding to interchain *d*-spacings of 20.91 and 18.70 Å, respectively. Fluorene−thiophene polymers **11** and **12** exhibit multiple diffraction features, with major features at $2\theta = 5.14°$ and 5.68°, corresponding to *d*-spacings of 17.17 and 15.54 Å, respectively, consistent with literature values assigned to interchain spacings (Figure S3).[90–94] In dithienosilole-based copolymers **6** and **7**, the absence of $\pi-\pi$ stacking diffraction features suggests that the polymer chains preferentially adopt layered structures with an "edge-on" orientation relative to the substrate, in analogy to the orientation of the $\pi-\pi$ stacks observed for regioregular P3HT, PQT-12, and PBTTT (Figure 2).[25,26,28] The dibenzosilole-based polymers exhibit broad peaks at ca. $2\theta = 20°$ for polymers **8** and **9** and at 21.95° for **10**, corresponding to $\pi-\pi$ stacking distances of

(83) Zhu, Y.; Alam, M. M.; Jenekhe, S. A. *Macromolecules* **2002**, *35*, 9844–9846.
(84) Zhu, Y.; Champion, R. D.; Jenekhe, S. A. *Macromolecules* **2006**, *39*, 8712–8719.
(85) Chua, L. L.; Zaumseil, J.; Chang, J. F.; Ou, E. C. W.; Ho, P. K. H.; Sirringhaus, H.; Friend, R. H. *Nature* **2005**, *434*, 194–199.
(86) Ohshita, J.; Nodono, M.; Kai, H.; Watanabe, T.; Kunai, A.; Komaguchi, K.; Shiotani, M.; Adachi, A.; Okita, K.; Harima, Y.; Yamashita, K.; Ishikawa, M. *Organometallics* **1999**, *18*, 1453–1459.
(87) Ohshita, J.; Nodono, M.; Watanabe, T.; Ueno, Y.; Kunai, A.; Harima, Y.; Yamashita, K.; Ishikawa, M. *J. Organomet. Chem.* **1998**, *553*, 487–491.
(88) Yamaguchi, S.; Xu, C. H.; Tamao, K. *J. Am. Chem. Soc.* **2003**, *125*, 13662–13663.
(89) Yang, S. Y.; Kan, Y. H.; Yang, G. C.; Su, Z. M.; Zhao, L. *Chem. Phys. Lett.* **2006**, *429*, 180–184.
(90) Grell, M.; Bradley, D. D. C.; Ungar, G.; Hill, J.; Whitehead, K. S. *Macromolecules* **1999**, *32*, 5810–5817.
(91) Kawana, S.; Durrell, M.; Lu, J.; Macdonald, J. E.; Grell, M.; Bradley, D. D. C.; Jukes, P. C.; Jones, R. A. L.; Bennett, S. L. *Polymer* **2002**, *43*, 1907–1913.
(92) Yamamoto, T.; Kokubo, H.; Morikita, T. *J. Polym. Sci., Part B: Polym. Phys.* **2001**, *39*, 1713–1718.
(93) Lim, E.; Jung, B. J.; Lee, J.; Shim, H. K.; Lee, J. I.; Yang, Y. S.; Do, L. M. *Macromolecules* **2005**, *38*, 4531–4535.
(94) Wu, Y.; Li, Y.; Gardner, S.; Ong, B. S. *J. Am. Chem. Soc.* **2005**, *127*, 614–618.

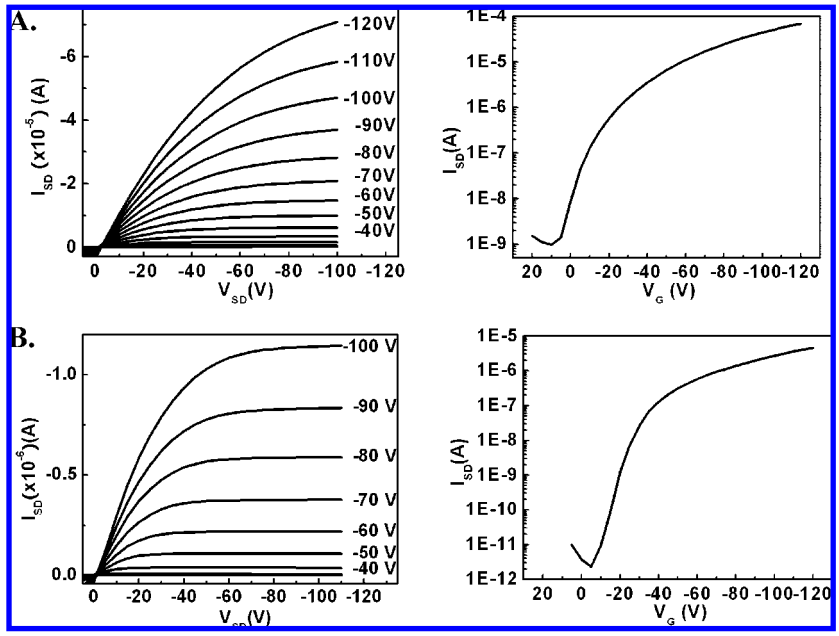

Figure 7. OTFT response plots of devices fabricated with polymers **7** and **10**. (A) Transfer plot of polymer **7** at $V_{SD} = -100$ V and output plot of polymer **7**. (B) Transfer plot of polymer **10** at $V_{SD} = -100$ V and output plot of polymer **10.**

4.0−4.4 Å, reminiscent of the distances measured previously for fluorene-based polymeric and oligomeric semiconductors.[93,94]

Transistor Fabrication and Optimization. OTFT devices were fabricated on low resistivity n-type silicon wafers, using thermally grown SiO_2 (300 nm) or hexamethyldisilazane (HMDS) passivated SiO_2 as the dielectric, in top-contact geometries. All device fabrication procedures were carried out in air. The active semiconducting layer was applied by spin-coating 5 mg/mL solutions in various solvents for 1 min. For top contact devices, gold contacts were patterned on top of the films using shadow masks that gave channel lengths of 25−100 μm and widths of 500−2000 μm. Devices fabricated with polymers **5** and **8** exhibit no FET activity. Devices fabricated with the remaining polymers were evaluated in ambient atmosphere as p-channel OTFTs in the accumulation regime. The output and transfer characteristics of devices fabricated with active polymers **6**, **7**, and **9**−**12** are presented in Figures 7 and S4.

To select the optimum solvent for thin-film growth, solutions of **6** and **7** in 1,2,4-trichlorobenzene (TCB, bp 214 °C), 1,4-dichlorobenzene (DCB, bp 180−181 °C), chlorobenzene (CB, bp 131 °C), *p*-xylene (bp 138 °C), and *o*-xylene (bp 143−145 °C) were spin-coated on silicon substrates with SiO_2 as the gate dielectric. Film thicknesses were 25−30 nm, as determined by profilometry. The solutions were heated to 80 °C to prevent gelation prior to spin coating. The resulting devices were annealed at 130 °C under nitrogen for 30 min before TFT measurements. It was found that 5 mg/mL solutions of **6** and **7** in the aforementioned solvents fail to form continuous thin films on HMDS-treated SiO_2/Si substrates. However, THF solutions of **6** and **7** form smooth thin films on the HMDS-treated SiO_2/Si substrates. In general, the TFT device performance of both polymers **6** and **7** on SiO_2/Si as the dielectric is poor in air. Additionally, the FET performance in general shows negligible dependence on the solvent boiling point. Devices of **6** spin-coated from 1,2-dichorobenzene exhibit the highest saturated hole mobility of 0.002 cm^2/V·s and $I_{on}/I_{off} \approx 10^2-10^3$ for a channel length of 100 μm, while hole mobilities are comparable for devices having films spin-coated from the other solvents. Thin films of polymer **7** spin-coated from all solvents exhibit very similar saturated hole mobilities of $\sim 10^{-4}$ cm^2/V·s. However, *p*-xylene and *o*-xylene are found to increase the I_{on}/I_{off} ratios for these devices by 1 order of magnitude for **7**. Devices fabricated from polymers **9** and **10** on untreated SiO_2 substrates show hole mobilities 1 to 2 orders of magnitude lower than those from devices fabricated with polymers **6** and **7**. Polymer **9** exhibits the lowest mobility of 5×10^{-6} cm^2/V·s with $I_{on}/I_{off} = 1 \times 10^4$ for thin films spin-coated from a TCB solution. Films of **10** provide the best overall performance for devices spin-coated from a TCB solution, with a mobility of 1×10^{-4} cm^2/V·s and $I_{on}/I_{off} = 1 \times 10^5$.

Devices fabricated with polymers **6**, **7**, **9**, and **10** spin-coated on HMDS-passivated SiO_2/Si substrates exhibit greatly enhanced TFT response. For polymers **6** and **7**, high-quality thin films can be obtained from hot THF solutions. This may be due to the low boiling point of THF compared to higher boiling solvents (1,2,4-trichlorobenzene, 1,4-dichlorobenzene, chlorobenzene, *p*-xylene), which facilitates smooth film growth on the highly hydrophobic HMDS surface before being spread during the spin-coating process. Film thicknesses were determined to be 25−30 nm by profilometry, with an rms roughness of 0.2−0.3 nm indicated by tapping mode AFM (for representative images, see Figure S5). After annealing at 150 °C under nitrogen, respective mobilities of 0.01 and 0.007 cm^2/V·s are obtained for **6** and **7**, with $I_{on}/I_{off} = 1 \times 10^4$ for both. The TFT performance of devices with polymers **9** and **10** is also enhanced by this processing methodology, yielding mobilities of 5×10^{-5} and 0.001 cm^2/V·s with I_{on}/I_{off} ratios of 3×10^4 and 4×10^5, respectively.

Thermal annealing is found to greatly improve the TFT performance for devices fabricated with polymers **6** and **7** (from THF) and **9** and **10** (from TCB), in terms of both mobility and I_{on}/I_{off} ratio. The devices were annealed under a nitrogen atmosphere at 100, 150, 200, 250, and 300 °C for 30 min, followed by cooling to room temperature by either quenching in air or slow cooling under nitrogen. In all cases, quenched

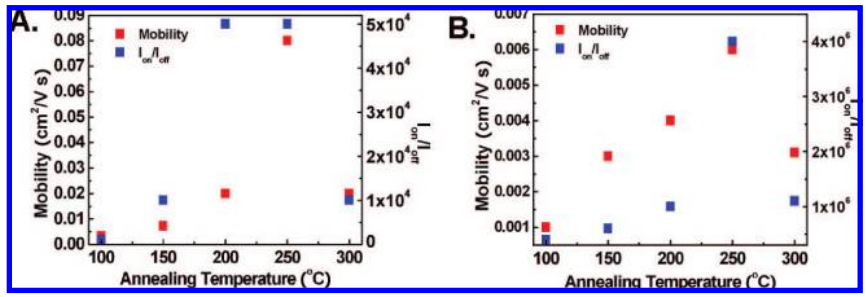

Figure 8. Evolution of field effect mobility and I_{on}/I_{off} ratio with annealing temperature in OTFTs fabricated with polymers **7** (A) and **10** (B).

devices have mobilities superior to those of slow-cooled devices. The evolution of mobility and I_{on}/I_{off} ratio for the present polymer devices is summarized in Figure 8. The performance maximizes at an annealing temperature of 250 °C (polymer **5** was annealed at 200 °C due to the lower decomposition temperature). For devices annealed at 250 °C, the highest mobilities of **6** and **7** are found to be 0.05 and 0.08 $cm^2/V\cdot s$, with I_{on}/I_{off} ratios of 1×10^5 and 5×10^4, respectively. For polymers **9** and **10**, the maximum mobilities are 6×10^{-5} and 0.006 $cm^2/V\cdot s$ with I_{on}/I_{off} ratios of 3×10^4 and 4×10^6, respectively. OTFT devices fabricated with fluorene-based copolymers exhibit hole mobilites of 9×10^{-5} $cm^2/V\cdot s$ with I_{on}/I_{off} ratios of 2×10^5 for **11** and 0.006 $cm^2/V\cdot s$ with I_{on}/I_{off} ratios of 2×10^5 for **12**. OTFT devices fabricated with polymers **6**, **7**, **10**, and **12** switch on crisply at around 0.0 V. For polymers **9** and **11**, the turn-on voltages are slightly greater (−10 to −30 V), probably because of the mismatch between the work function of the gold electrode (−5.1 V) and the polymer HOMO levels (*vide infra*). Higher annealing temperatures are found to have detrimental effects on all of the present polymers, even though the T_m's of **7** and **10** are ∼300 °C. This may reflect the formation of segregated rods consisting of $\pi-\pi$-stacked polymer lamella that plausibly inhibit efficient charge transfer.[95]

Printed OFETs were fabricated with polymer thin films deposited by gravure printing from a highly viscous solution of **10** (0.5 wt % in TCB) on a PET-Al-CPB substrate (CPB = cross-linked polymer blend[96]) in which the dielectric layer is also printed (∼20 wt % in AcOEt). After printing and before Au source/drain contact deposition, the printed films were annealed at ∼100 °C for 30 min under vacuum. The printed devices exhibit a saturated hole mobility of $10^{-4}-10^{-5}$ $cm^2/V\cdot s$ and $I_{on}/I_{off} \approx 100$ when measured in air (Figure S6). Although the mobility values for these gravure-printed devices are lower than those for spin-coated films, all of the devices function reproducibly as p-channel transistors, which is remarkable considering the simplicity of the gravure printing technique and low annealing temperature. We believe that FET performance can be further improved by optimizing the printing conditions.

Device Air Stability. OFETs fabricated using materials **6**, **7**, **9**, and **10** operate well in air, exhibiting very good ambient storage stability and electrical stability. The stability of the polymer devices stored in air without exclusion of light and humidity was evaluated over a period of time. The off currents of devices fabricated with **7** and exposed to air for 3 weeks increase by less than 1 order of magnitude, while the on current remains unchanged (Figure 9A). The I_{on}/I_{off} ratios of **10**-based TFTs decline by less than 1 order of magnitude after 60 days (Figure 9C). In both cases, nearly identical threshold voltages, mobilities and I_{on}/I_{off} ratios are obtained, demonstrating excellent air stability for devices made from polymers **7** and **10**. After 1 year of storage under ambient conditions, including laboratory exposure to light, the I_{on}/I_{off} ratios are found to be in a range of $\sim 1 \times 10-5 \times 10^3$. The positive shift in threshold voltage after a few weeks can be attributed to slight p-doping by O_2.[42] Negative shifts in threshold voltage observed after prolonged ambient storage have previously been attributed to many effects, including charge trapping at the semiconductor-dielectric interface and bipolaron formation within the semiconductor.[42] For comparison, OTFTs of the well-known semiconducting polymer P3HT were fabricated under the same conditions as **7** and **10**. The FET performance of P3HT was found to be very sensitive to air. When measured in vacuum, the devices exhibit an average initial I_{on}/I_{off} ratio of $\sim 10^4$ which drops to less than 10^2 when the devices are exposed to air (Figure 9E), consistent with previous reports.[94] OTFT electrical stability was also tested by repeatedly switching the device on and off in air at various gate biases. For both **7** and **10**, the OTFT performance shows little indication of degradation, with I_{on}/I_{off} ratios at a fixed gate voltage remaining essentially constant (Figure 9B and 9D).

Discussion

Polymer Architecture vs FET Performance. In general, dithienosilole copolymers **6** and **7** exhibit larger hole mobilities than the corresponding dibenzosilole copolymers **9** and **10**, while bithiophene copolymers **7** and **10** have greater hole mobilities than thiophene copolymers **6** and **9**. Those factors affecting semiconducting polymer film mobilities reflect a complex interplay of electronic structure, injection, trapping, charge transfer parameters, polymer molecular weight,[95,97] and side-chain regioregularity,[25] as well as macromolecular crystallinity and morphology.[98] Optimization of the molecular weights of the present polymers was attempted by using several polymerization protocols (*vide supra*). Additionally, side-chain regioregularity is not relevant here because the silole cores are symmetrical. Thus, the performance of devices fabricated with polymers **5**−**12** in this contribution appears to be primarily dependent on polymer crystallinity, morphology, and injection barriers.

Dithienosilole homopolymer **5** exhibits no diffraction features, even after annealing, revealing poor or no crystal-

(95) Kline, R. J.; McGehee, M. D.; Kadnikova, E. N.; Liu, J. S.; Frechet, J. M. J.; Toney, M. F. *Macromolecules* **2005**, *38*, 3312–3319.
(96) Facchetti, A.; Yoon, M. H.; Marks, T. J. *Adv. Mater.* **2005**, *17*, 1705–1725.
(97) Zen, A.; Saphiannikova, M.; Neher, D.; Grenzer, J.; Grigorian, S.; Pietsch, U.; Asawapirom, U.; Janietz, S.; Scherf, U.; Lieberwirth, I.; Wegner, G. *Macromolecules* **2006**, *39*, 2162–2171.
(98) Yang, H. C.; Shin, T. J.; Yang, L.; Cho, K.; Ryu, C. Y.; Bao, Z. N. *Adv. Funct. Mater.* **2005**, *15*, 671–676.

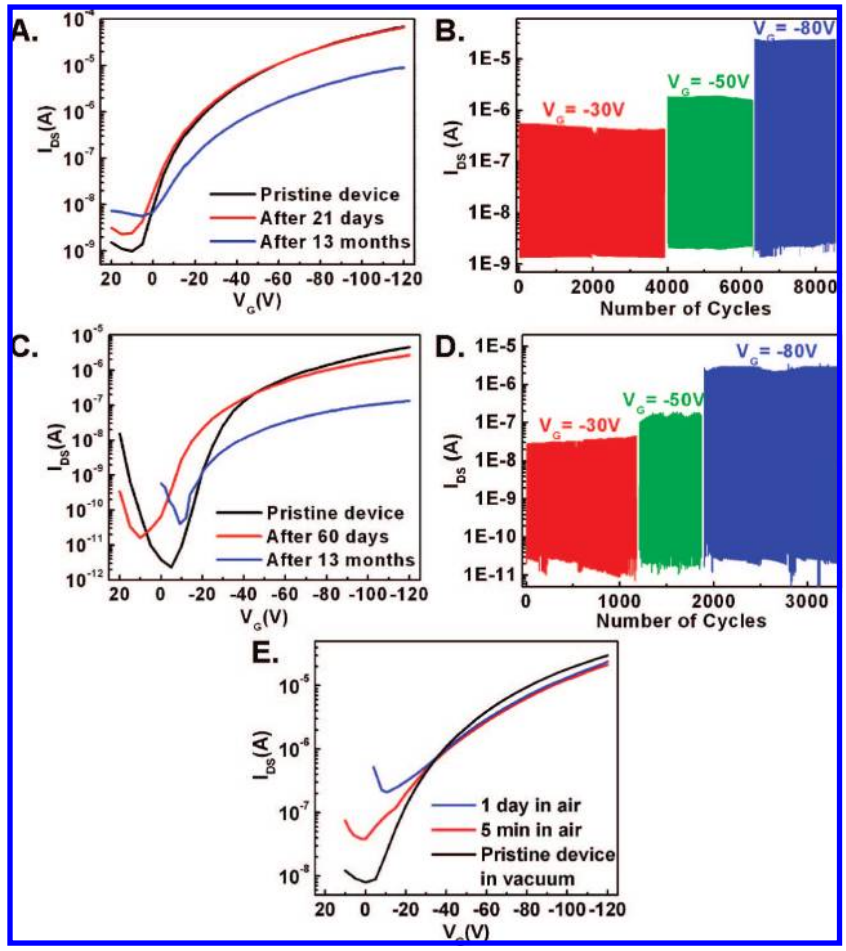

Figure 9. Transfer characteristics of OTFT devices fabricated with polymers **7** (A), **10** (C), and **P3HT** (E) as a function of storage time in the air. The on−off cycles (0.03 Hz) under ambient conditions for the annealed devices fabricated with polymers **7** (B) and **10** (D) at $V_{SD} = -50$ V were measured for the different gate biases indicated.

linity, and is found to be FET-inactive. In contrast, polymers **6**, **7**, and **10** exhibit high FET saturated hole carrier mobilities when measured in air, most likely a consequence of the high level of molecular organization, namely crystallinity, of these polymers in the solid state as evidenced by the XRD data (Figure 6). Without annealing, thin films of polymers **6** and **7** are amorphous and have poor hole mobilities. However, they exhibit high-crystallinity diffraction patterns after annealing at 250 °C, each pattern having three equally spaced reflections assignable to members of the same Bragg family. Importantly, the mobility of these two polymers increases as the annealing temperature is increased and maximizes at ∼250 °C (Figure 8). Similar results are obtained for polymers **9** and **10**. These results argue that the degree of crystallinity is, not unexpectedly, a major factor determining the measured carrier mobility in these polymers. Judging from the number of reflections, fwhm values, and diffraction peak intensities, polymer **7** is the most crystalline of the three dithienosilole polymers. The crystallinity decreases on proceeding from **7** to **6** to **5**, apparent in the XRD spectra, and correlates with the observed trend in carrier mobilities. In addition to the high degree of crystallinity, the preferential "edge-on" orientation of polymers **6** and **7** relative to the substrate may lead to layered structure formation with the $\pi-\pi$ stacking direction parallel to the substrate plane, which is known to favor in-plane source-to-drain (S → D) charge transport (as in Figure 2).[25] By the same token, among polymers **8**, **9**, and **10**, polymer **10** appears to have the greatest crystallinity, correlating with enhanced mobility.

The trend in the melting points of the present polymers (see Table 1) is in accord with the observed increase in carrier mobility from the monothiophene to bithiophene copolymers. For polymers **6** and **7**, the melting point increases by ∼40 °C, while, for polymers **9** and **10**, the increase is even more substantial (∼90 °C). The elevated melting points of the bithiophene polymers, given the architectural similarity of the polymers, suggest that these macromolecules may be more densely packed in the solid state. For polymers **6** and **7**, the interchain lamellar *d*-spacings (15.54 and 15.38 Å, respectively) are somewhat smaller than twice the distance from the end of the *n*-hexyl group to the sulfur atoms of the silole core obtained in the DFT calculations (9.1 Å; Figure 10A, see below), suggesting that the polymer chains likely assume an interdigitated packing motif similar to that in P3HT thin films[25] (Figure 2), although the precise orientation of the alkyl chains cannot be determined with the present XRD data alone. The interchain distances are somewhat shorter than that of P3HT (16.8 Å)[25] but much longer than that of PQT-12 (12 Å; Figure 2).[28] Polymers **9** and **10** exhibit larger spacings

(99) Zhang, R.; Li, B.; Iovu, M. C.; Jeffries-EL, M.; Sauve, G.; Cooper, J.; Jia, S. J.; Tristram-Nagle, S.; Smilgies, D. M.; Lambeth, D. N.; McCullough, R. D.; Kowalewski, T. *J. Am. Chem. Soc.* **2006**, *128*, 3480–3481.

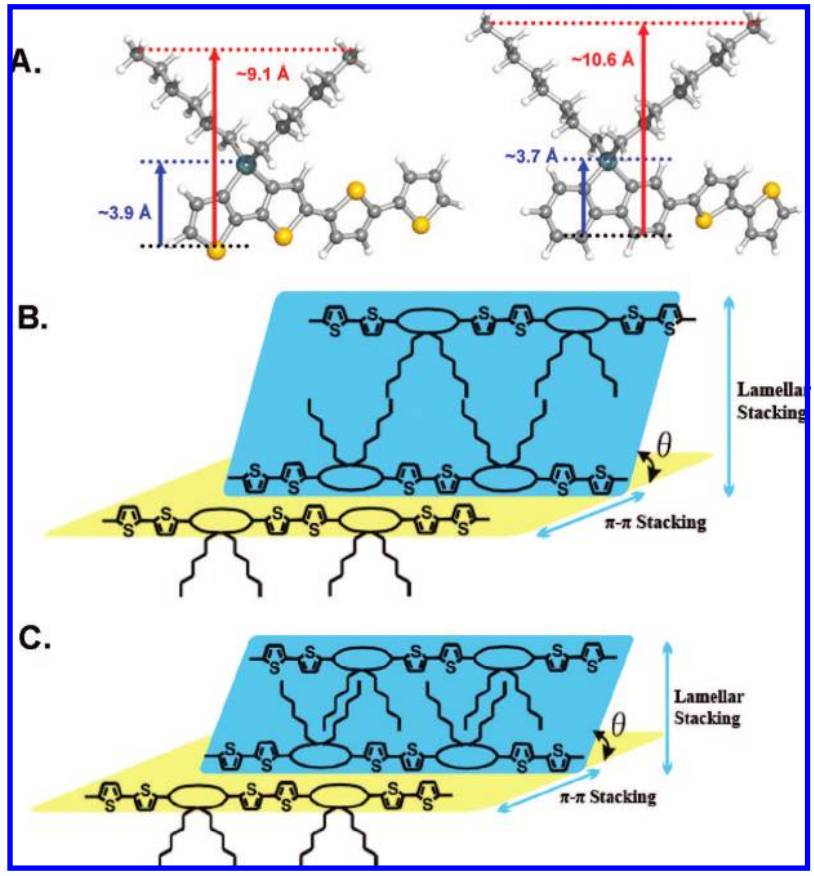

Figure 10. Schematic models of layered and $\pi-\pi$ stacked silole copolymer structures **7** and **10**: DFT-calculated molecular dimensions (A), no side chain interdigitation model (B), and minimal free volume model (C).

(20.91 and 18.70 Å, respectively), which are *ca.* 3 Å longer than the previously reported layer periodicities of ~15−17 Å observed for alkyl-substituted fluorene and carbazole-based polymers and related small molecules.[93,94,100]

These distances are also slightly smaller than twice the distance from the end of the *n*-octyl groups to the edge-carbon atoms of the silole core obtained from the DFT calculation (10.6 Å; Figure 10A). The *d*-spacing values of copolymers **6**, **7**, **9**, and **10** suggest that the *n*-hexyl and *n*-octyl side chains may interdigitate. Two possible packing motifs are depicted in Figure 10B and 10C. Figure 10B shows a model in which the alkyl side chains do not interdigitate. In the horizontal plane, the polymer backbones are roughly perpendicular to the substrate with a tilt angle θ, and the electron-deficient silole cores overlap with bithiophene moieties. The alkyl side chains of each unit in the polymer are perpendicular to the substrate, consistent with the edge-on polymer orientation evidenced by the diffraction data. In the second model (Figure 10C), the polymer alkyl side chains interdigitate to some extent in the vertical plane. These models illustrate two extreme cases of the polymer thin-film microstructure, with the tilt angle highly dependent on the extent of side chain interdigitation for a given *d*-spacing.

Optical spectroscopy also provides polymer structural information both in solution and in the solid state. In general across the series, the addition of thiophene rings to the polymer backbone induces a red-shift in the solution optical absorption (a result in agreement with DFT calculations, *vide infra*). The one anomaly in the series is homopolymer **5** which exhibits a red-shifted absorption maximum vs monothiophene-substituted **6** in THF. This result for **5** may reflect aggregation in solution, as evidenced by the strong shoulder around 400 nm;[101,102] in the solid state, the shoulder disappears after vacuum annealing, indicating the elimination of this aggregation pattern in the solid state. The optical absorption maximum of polymer **6** red-shifts ~50 nm on going from solution to thin films, suggesting that, in the solid state, polymer **6** achieves a higher degree of molecular organization than in solution. For polymers **7**, **9**−**12**, the absorption spectra of the thin films are generally similar in vibronic pattern and shape to those in dilute solutions, indicating comparable ground-state electronic structures and similar backbone conformations in the solution and solid states.

Electrochemical and Optical Properties as a Function of Electronic Structure. The solution and solid-state optical absorption data, along with the electrochemical oxidation potentials, reveal an important role for the heteroatom substitutions in the arylene backbones of the present polymer chains. To understand better the evolution of electronic states and ionization energies with substitution, electronic structure calculations at the density functional theory (DFT) level were carried out to model the polymer building blocks (Figure 11); note here that the 1,1′-substituents on each of the model fragments are methyl groups to simulate the influence of alkyl

(100) Boudreault, P.-L. T.; Wakim, S.; Blouin, N.; Simard, M.; Tessier, C.; Tao, Y.; Leclerc, M. *J. Am. Chem. Soc.* **2007**, *129*, 9125–9136.

(101) Koren, A. B.; Curtis, M. D.; Kampf, J. W. *Chem. Mater.* **2000**, *12*, 1519–1522.

(102) Yamamoto, T.; Komarudin, D.; Arai, M.; Lee, B. L.; Suganuma, H.; Asakawa, N.; Inoue, Y.; Kubota, K.; Sasaki, S.; Fukuda, T.; Matsuda, H. *J. Am. Chem. Soc.* **1998**, *120*, 2047–2058.

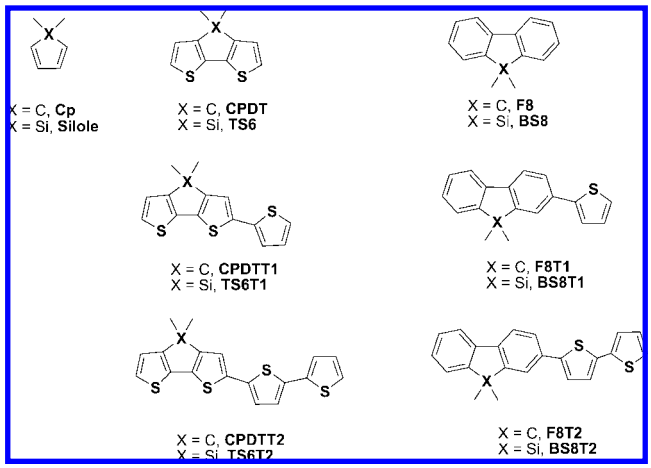

Figure 11. Chemical structures of model polymer building blocks for electronic structure calculations.

chains on the geometric and electronic structure properties of each arylene. Selected molecular orbital energies, low-lying singlet state energies, and the corresponding excited-state configurations are compiled in Table 3, while Figure 12 provides contour representations of selected valence MOs for the model fragments. For the three pairs of aromatic cores compared (cyclopentadiene/silole, F8/BS8, and CPDT/TS6), introduction of Si into the molecular structures energetically stabilizes both the HOMO and LUMO, with the LUMO undergoing more significant stabilization, in accord with previous theoretical analyses of related, nonsemiconductor systems.[89,103] With no significant π-orbital character for either the central C or Si of the aromatic cores, the minimal stabilization of the HOMO in the Si-containing species is a result of the larger Si atom size, which leads to increased bond lengths to the nearest neighbor atoms by ~0.36 Å vs the C analogue, and in turn decreases antibonding interactions within the *cis*-butadiene-like HOMO. In contrast, the more significant LUMO stabilization reflects the extended conjugation from the overlap between the two exocyclic Si−C bond σ^*-orbitals and the butadiene moiety π^*-orbital; in contrast, the $2p_z$-orbitals of the C-analogues are too energetically destabilized to effectively participate in such bonding.[103] This interaction is often invoked to explain the large electron affinities of siloles vs their cyclopentadiene analogues.[103,104]

Subsequent introduction of thiophene rings to represent more accurately the mono- and bithiophene units of the complete polymers (Figure 11) leads to energetic destabilization of the HOMO and stabilization of the LUMO with each new thiophene unit; the HOMO and LUMO wave function densities for these monomeric systems are delocalized across the molecular structures.[105] Note that the comparative HOMO and LUMO energies for dithieno- and dibenzo-, C- and Si-substituted structures are nearly identical, a result not expected *a priori* considering the aforementioned core unit trends. Inspection of the HOMO densities for these systems shows that the wave functions are delocalized in the same manner across the structures and are linear combinations of the core HOMO with the thiophene HOMO. Using Koopmans' theorem, the DFT-derived HOMO energetic trends (Table 3) track the electrochemically obtained oxidation potentials well (Table 2). As a complement to the ionization energies obtained from the electrochemical (adiabatic) measurements, direct adiabatic ionization potential and electron affinity calculations for the model building blocks were also performed (Table 3). These results reveal that Si atom inclusion in the arylene backbone makes a negligible contribution to the fragment oxidation energies, in agreement with the computed frontier orbitals. Increasing the number of (closed shell) thiophene units in the monomer decreases the ionization energy, thus providing an additional mechanism for stabilization of the oxidation products. As with the HOMO energies, the adiabatic ionization potentials track the estimated IP^{ox} values well (see Figure 13A); the difference in absolute values between the calculated and experimentally estimated values is not surprising in that (i) the calculations are performed for small model monomers while the experimental data are for full polymer chains and (ii) there exist inherent limitations (e.g., solvent polarity effects) in using eq 1 to estimate gas-phase ionization potentials for polymers.

In a fashion analogous to the thiophene-containing monomer HOMOs, the C- and Si-substituted monomer LUMO π^*-densities are similar (Figures 12). For the Si-containing systems, there is no significant electron density found on the Si atom in the LUMO for any of the thiophene-substituted systems; this is in direct contrast to what was observed for the smaller aryl cores (*vide supra*) and other previously investigated silole-like systems.[48,49,106] Incorporation of the thiophene units into the present structures increases the conjugation length of the carbon backbone, leading to energetic stabilization of the carbon-backbone-based π^*-orbital, thereby reducing the $\sigma^*-\pi^*$ interaction typically observed in silole structure LUMOs.[48,49,106] These $\sigma^*-\pi^*$ interactions are not observed until the LUMO+1 levels, which lie appreciably higher in energy (on the order of 0.7−1.2 eV) above the LUMOs in these molecules; inspection of the Si atomic orbital coefficients in the LUMO and LUMO+1 levels reveals a much larger contribution to LUMO+1. These results therefore suggest that reduction of these species may be energetically more demanding, compared to their carbon analogues, than typical siloles due to the loss of the extended LUMO conjugation. Indeed, the computed LUMO energies are virtually identical for the Si- and C-containing species, thus suggesting that the reductive properties of these materials should be similar (more so than for the core aryl structures, *vide supra*). Directly calculated adiabatic electron affinities for the dithienosilole/cyclopentadiene and dibenzosilole/cyclopentadiene pairs (Table 3) confirm this assessment. While there is substantial correspondence between the LUMO energies and the electrochemically derived EA^{ox} values, the agreement between the theoretical and experimental data is not as close as that for the ionization potentials. Overall, the frontier orbital energies and calculated ionization energies are consistent with the observed polymer electrochemical characterization, where no clear reductive properties are observed although reversible and irreversible oxidative features are detected.

Using the electronic structures of the model building blocks and the time-dependent DFT (TDDFT) formalism, the lowest-lying excited-state energies are found to track the computed HOMO−LUMO gaps closely (see Table 3). The principal

(103) Yamaguchi, S.; Itami, Y.; Tamao, K. *Organometallics* **1998**, *17*, 4910–4916.
(104) Faustov, V. I.; Egorov, M. P.; Nefedov, O. M.; Molin, Y. N. *Phys. Chem. Chem. Phys.* **2000**, *2*, 4293–4297.
(105) Belletête, M.; Beaupré, S.; Bouchard, J.; Blondin, P.; Leclerc, M.; Durocher, G. *J. Phys. Chem. B* **2000**, *104*, 9118–9125.
(106) Yamaguchi, S.; Tamao, K. *J. Chem. Soc., Dalton Trans.* **1998**, 3693–3702.

Table 3. Computed Adiabatic Ionization Potentials and Electron Affinities (eV), Selected Valence Molecular Orbital Energies (eV), HOMO−LUMO Gaps (eV), Low-Lying Excited-State Energies (eV and nm, in Parentheses), Oscillator Strengths, and Excited-State Configurations As Determined at the B3LYP/6-31G** Level

compound	AIP[a]	AEA[a]	HOMO	LUMO	E_g	λ	osc. str.	configuration
cyclopentadiene	7.76	1.55	−5.70	−0.34	5.36	5.01 (247)	0.05	HOMO → LUMO (99%)
silole	7.87	0.64	−5.96	−1.09	4.87	4.39 (283)	0.05	HOMO → LUMO (99%)
F8	7.28	0.72	−5.74	−0.76	4.98	4.62 (269)	0.27	HOMO-2 → LUMO (11%); HOMO → LUMO (71%); HOMO → LUMO+1 (13%)
						4.77 (260)	0.09	HOMO-2 → LUMO (15%); HOMO → LUMO (23%); HOMO → LUMO+1 (61%)
F8T1 (**11**)	6.66	−0.03	−5.40	−1.24	4.16	3.87 (321)	0.84	HOMO → LUMO (99%)
F8T2 (**12**)	6.24	−0.52	−5.15	−1.56	3.59	3.30 (376)	1.21	HOMO → LUMO (99%)
BS8 (**8**)	7.27	0.45	−5.79	−0.93	4.85	4.30 (288)	0.08	HOMO → LUMO (74%); HOMO → LUMO+1 (20%)
						4.60 (270)	0.13	HOMO-1 → LUMO (30%); HOMO → LUMO (21%); HOMO → LUMO+1 (47%)
BS8T1 (**9**)	6.65	−0.13	−5.42	−1.32	4.10	3.76 (330)	0.62	HOMO → LUMO (97%)
						4.14 (300)	0.14	HOMO-2 → LUMO (8%); HOMO → LUMO+1 (80%)
BS8T2 (**10**)	6.23	−0.58	−5.15	−1.60	3.55	3.26 (381)	1.16	HOMO → LUMO (99%)
						3.86 (322)	0.04	HOMO-1 → LUMO (6%); HOMO → LUMO+1 (79%); HOMO → LUMO+2 (8%)
CPDT	6.73	0.49	−5.19	−1.02	4.17	3.93 (316)	0.31	HOMO → LUMO (99%)
CPDTT1	6.20	−0.26	−4.90	−1.54	3.36	3.18 (389)	0.75	HOMO → LUMO (100%)
CPDTT2	5.91	−0.69	−4.80	−1.79	3.01	2.82 (440)	1.16	HOMO → LUMO (100%)
						3.96 (313)	0.02	HOMO-1 → LUMO (67%); HOMO → LUMO+2 (31%)
TS6 (**5**)	6.77	0.13	−5.30	−1.29	4.00	3.63 (341)	0.23	HOMO → LUMO (99%)
TS6T1 (**6**)	6.23	−0.42	−4.98	−1.66	3.32	3.07 (404)	0.60	HOMO → LUMO (99%)
						3.95 (314)	0.06	HOMO-1 → LUMO (16%); HOMO → LUMO+1 (80%)
TS6T2 (**7**)	5.94	−0.78	−4.86	−1.85	3.01	2.78 (447)	1.05	HOMO → LUMO (99%)
						3.39 (365)	0.04	HOMO-1 → LUMO (17%); HOMO → LUMO+1 (80%)
						3.82 (325)	0.03	HOMO-1 → LUMO (80%); HOMO → LUMO+1 (16%)

[a] Computed using ΔSCF methods.

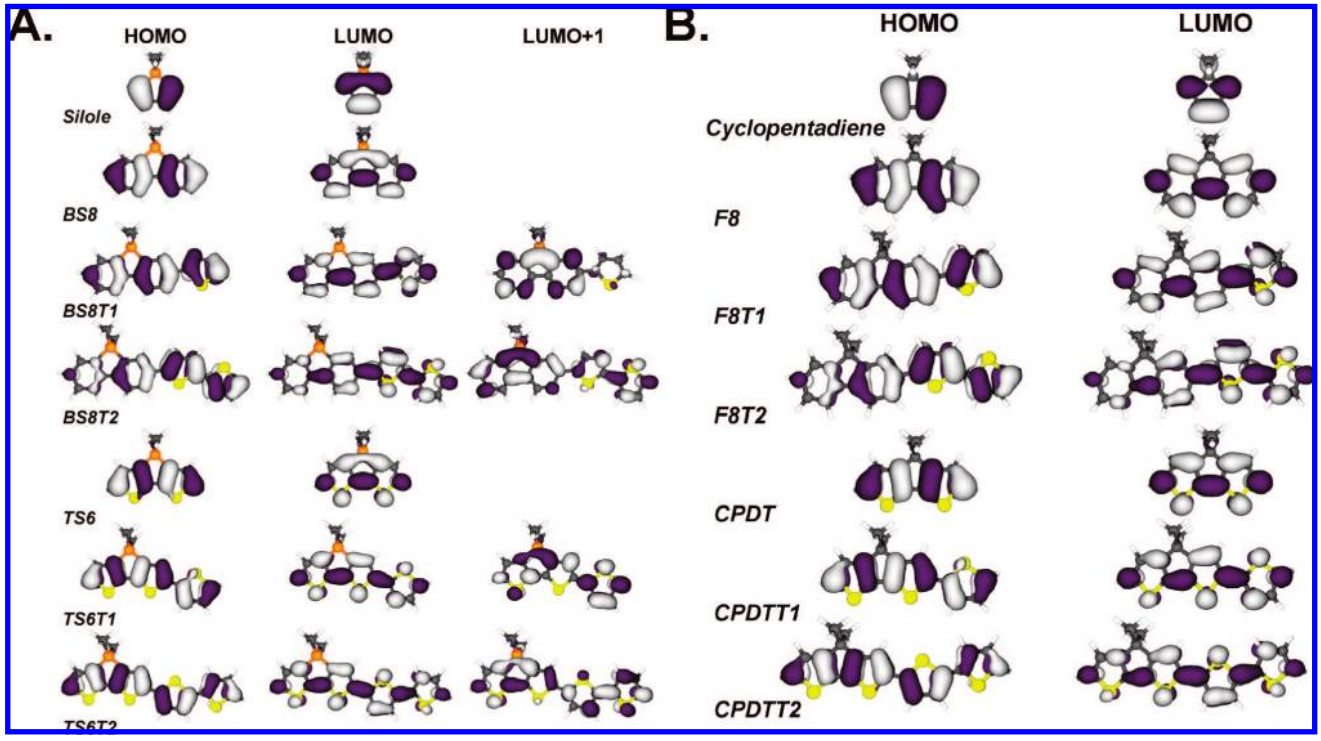

Figure 12. Pictorial representations of B3LYP/6−31G**-derived selected valence molecular orbitals for the present silole-based polymer building blocks (A) and carbon-based polymer building blocks (B).

transition for each model fragment is characterized as being predominantly HOMO → LUMO in character, with minor transitions involving other nearby valence MOs. The calculated excited-state energies for the model fragments exhibit optical absorption maxima red-shifts with increasing thiophene substitution and also on going from dibenzosilole- to dithienosilole-based polymers. These trends agree well with both the experimental solution and thin-film absorption properties for the polymers (Table 1).

Role of the Injection Barrier. In addition to microstructural and morphological differences among the present polymers in the solid state, there are also expected differences in the hole injection barriers from the gold electrodes to the polymer HOMO (see Figure 13) that likely affect OFET performance

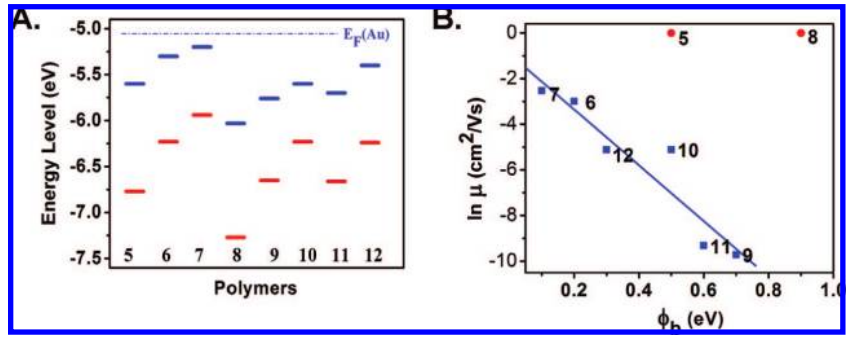

Figure 13. (A) Comparison of theoretical (AIP, red) and experimentally estimated (IP^{ox}, blue) ionization potentials using eq 1; differences in the ionization potentials for each species arise from a comparison of a model monomer (theoretical) versus the full polymer (experimental) measurements and neglect solvent dielectric effects in the gas-phase calculations. (B) Experimental FET mobility as a function of hole injection barrier. Note that for polymers **5** and **8** negligible mobilities were measured.

by altering contact resistance and turn-on voltage.[107–109] According to a simple Schottky-type charge injection barrier model, the relative hole injection rates for a series of related materials should have an exponential dependence on the hole injection barrier, Φ_B, assumed to be the difference between the metal electrode Fermi level (E_F) and the polymer ionization potential (eq 2).[16,110,111]

$$\Phi_B = E_F - IP \quad (2)$$

Note that, for the estimates that follow, we use the electrochemical estimate of the ionization potential, IP^{ox}. Assuming a gold Fermi level energy of 5.1 eV,[85] Φ_B is expected to be small (~0.2 eV) for the dithienosilole-based copolymers **6** and **7**. OTFTs fabricated with polymers **6** and **7** switch on crisply at ~0 V, indicative of a small Φ_B. For electron-deficient dibenzosilole-based copolymers **9** and **10**, the estimated injection barriers are significantly greater at 0.7 and 0.5 eV, respectively. Note that these polymers exhibit significantly higher turn-on voltages of −10 to −20 V, probably reflecting, among many factors, these differences in injection barriers. Fluorene-based copolymers **11** and **12** exhibit similar trends in that a high energy level offset for **11** (0.6 eV) results in higher OTFT turn-on voltages of −20 to −30 V, whereas devices fabricated with **12** have low turn-on voltages of 0 V to −5 V, in agreement with the smaller energy level mismatch of ~0.3 eV. Some detectable contact resistance due to the high injection barriers is also evident for polymers **9** and **11** as slight curvatures in the source−drain current plot at low source−drain voltages in the output curves (Figure S4).

We note interestingly that, without exception across the present polymer series, a direct correlation exists between the hole injection barrier Φ_B and FET hole mobility μ_h (Figure 13B): polymers **6**, **7**, **10**, and **12** are shown to have small injection barriers and large measured mobilities, while polymers **5** and **8** (inactive as semiconductors),[107,112] **9**, and **11** have larger injection barriers and small measured mobilities. These results suggest that injection barriers not only play a critical role in turn-on voltage and contact resistance for these polymers but also affect the measured TFT hole transport characteristics, a result that we also observed recently for a series of carbonyl-functionalized quarterthiophene (n-type, μ_e) organic semiconductors.[113] Charge transport models that consider charge injection via a thermally activated injection process (as we have done throughout) into a disordered medium—whether one considers the current to be solely injection-limited (ILC)[114] or that there exists an interplay between ILC and space charge-limited current (SCLC)[115–118]—suggest that the size of Φ_B can indeed have a profound impact on the measured current and, hence, measured μ_h in organic semiconducting systems. For these polymers, further temperature- and field-dependent studies will be required to discern further details of the limiting charge transport mechanism.

Conclusions

We have synthesized and characterized a new family of silole-containing polymers, **5**−**10**. For comparison, fluorene−thiophene copolymers **11** (investigated for the first time here in an OTFT) and **12** were also synthesized. Polymers **5**−**12** have excellent thermal and environmental stability. Polymers **5** and **8** are found to be FET-inactive, probably because of poor film-forming tendencies and substantial hole injection barriers. Monothiophene-containing copolymers **6**, **9**, and **11** are p-channel materials, with **9** and **11** exhibiting moderate hole mobilities of $\sim 10^{-4}$ $cm^2/V \cdot s$. Polymer **6** exhibits a substantial hole mobility of 0.05 $cm^2/V \cdot s$ in air, with an I_{on}/I_{off} ratio of 1×10^5. Bithiophene-containing copolymers **7**, **10**, and **12** are also found to be p-channel materials with excellent OTFT performance. For polymer **7**, hole mobilities up to 0.08 $cm^2/V \cdot s$ with an I_{on}/I_{off} ratio $> 5 \times 10^4$ are achieved under ambient conditions with a near-zero turn-on voltage. For polymer **10**, a hole mobility of 6.0×10^{-3} $cm^2/V \cdot s$ is obtained with a maximum current on/

(107) Liao, L. S.; Fung, M. K.; Lee, C. S.; Lee, S. T.; Inbasekaran, M.; Woo, E. P.; Wu, W. W. *Appl. Phys. Lett.* **2000**, *76*, 3582–3584.
(108) Heeney, M.; Bailey, C.; Giles, M.; Shkunov, M.; Sparrowe, D.; Tierney, S.; Zhang, W. M.; McCulloch, I. *Macromolecules* **2004**, *37*, 5250–5256.
(109) Bürgi, L.; Richards, T. J.; Friend, R. H.; Sirringhaus, H. *J. Appl. Phys.* **2003**, *94*, 6129–6137.
(110) Chwang, A. B.; Frisbie, C. D. *J. Phys. Chem. B* **2000**, *104*, 12202–12209.
(111) Mahapatro, A. K.; Ghosh, S. *Appl. Phys. Lett.* **2002**, *80*, 4840–4842.
(112) Janietz, S.; Bradley, D. D. C.; Grell, M.; Giebeler, C.; Inbasekaran, M.; Woo, E. P. *Appl. Phys. Lett.* **1998**, *73*, 2453–2455.
(113) Yoon, M. H.; DiBenedetto, S. A.; Russell, M. T.; Facchetti, A.; Marks, T. J. *Chem. Mater.* **2007**, *19*, 4864–4881.
(114) Burin, A. L.; Ratner, M. A. In *Computational Materials Chemistry: Methods and Applications*; Curtiss, L. A., Gorden, M. S., Eds.; Kluwer Academic Publishers: The Netherlands, 2004; pp 308−367.
(115) Arkhipov, V. I.; Emelianova, E. V.; Tak, Y. H.; Bässler, H. *J. Appl. Phys.* **1998**, 84.
(116) Arkhipov, V. I.; Wolf, U.; Bässler, H. *Phys. Rev. B* **1999**, *59*, 7514–7520.
(117) Arkhipov, V. I.; Seggern, H. v.; Emelianova, E. V. *Appl. Phys. Lett.* **2003**, *83*, 5074–5076.
(118) Zheng, Y.; Kunardi, L.; Troadec, C.; Wee, A. T. S.; Chandrasekhar, N. *Appl. Surf. Sci.* **2006**, *252*, 4023–4025.

off ratio of 4×10^6. OTFTs fabricated using polymers **7** and **10** are very stable upon exposure to ambient air and light. DFT calculations indicate that silicon substitution stabilizes both the HOMO and LUMO levels of the dithienosilole and dibenzosilole cores, rendering the silole copolymers less susceptible to O_2 doping. The theoretical and optical characterization data suggest high degrees of π-delocalization in the silole-based polymers with increased ionization potentials and electron affinities vs the carbon counterparts. We also observe and discuss a direct correlation between hole injection barriers and both the OTFT measured turn-on voltages and hole mobilities. These results, in total, affirm the possibility of achieving low-cost microelectronic devices through organic materials that enable simple solution fabrication processes under ambient conditions.

Acknowledgment. We thank ONR (N00014-05-1-0766) and AFOSR (STTRFA 9550-04-0080) for support of this research, and the NSF-MRSEC program through the Northwestern University Materials Research Science and Engineering Center (DMR-0520513) for providing both support and characterization facilities.

Supporting Information Available: Synthetic procedures of dibenzosilole and dithienosilole monomers and polymers (**16**, **17**, **21**, **22**, and **5**−**12**); thermogravimetric analysis (TGA) and differential scanning calorimetry (DSC) plots of the polymers **5**−**12**; $\theta-2\theta$ X-ray diffraction (XRD) scans of drop-cast films of polymers **11** and **12**; OFET plots of devices fabricated with polymers **6**, **9**, **11**, and **12**; AFM images of the thin-films of polymer **10**; transfer and output plots of printed OFET devices fabricated with polymer **10**. This material is available free of charge via the Internet at http://pubs.acs.org.

JA800424M